Master of Science Thesis

Behaviour of Suction Caisson subjected to Cyclic Loading in Tension

Kamaleshwar Sudhakaran

TU Delft Delft University of Technology

Behaviour of Suction Caisson subjected to Cyclic Loading in Tension

Master of Science Thesis

For obtaining the degree of Master of Science in Civil Engineering
at Delft University of Technology

Kamaleshwar Sudhakaran

Student Number: 4607287

December 2018

Delft University of Technology
Faculty of civil engineering and applied earth sciences
Department of Civil engineering (Geo-engineering)

GRADUATION COMMITTEE

Supervisor:

Dr. Amin Askarinejad
Assistant Professor,
Geo-engineering section,
Delft University of Technology

Thesis committee:

Dr. Ken Gavin
Professor of Subsurface engineering,
Geo-engineering section,
Delft University of Technology

Dr. Robert Lanzafame
Lecturer,
Hydraulic structure and Flood risk,
Delft University of Technology

Dr. Vahid Galavi
Senior consultant/researcher,
Deltares, Delft.

Acknowledgement

This thesis comprises of a 9 month long research conducted at the Geo-engineering section of Delft University of Technology, as a final part of my Master of Science degree in Civil engineering.

I am grateful to my supervisor Dr. Amin Askarinejad for providing me with this opportunity and giving me the freedom to do the research independently. His guidance, advice and timely discussions throughout the thesis were very valuable to me and pushed me to achieve higher standards.

I would like to thank Dr. Vahid Galavi for helping me out with Plaxis modelling and providing me with some key knowledge regarding UBC sand model. My sincere thanks to Dr. Robert Lanzafame for being a part of my committee and also for allocating the time to give valuable comments on my presentation and thesis report. I would also like to thank Dr. Ken Gavin for agreeing to be in my committee.

I could not have assembled the suction installation apparatus on my own and for that I would like to express my deepest gratitude to Han De Visser, Kees Van Beek and Ron. I would like to thank Sathish for helping me out with the matlab code and Revathy, Madhumitha and Anjana for proofreading my report.

Finally, I would like to thank my dad and mom for always being there for me and supporting me to obtain this masters degree. I would also like to thank my grandfather Selvaraj and grandmother Indhu for everything they have done for me. I am forever indebted to them for that.

Kamaleshwar Sudhakaran
Delft, December 2018

Abstract

As countries around the world are in a race for clean energy, various renewable energy sources are harvested to meet the energy needs. In Western Europe, wind energy is the primary source of renewable energy. To meet the energy demand, higher capacity wind turbines are being installed in deeper waters. In deep waters, monopile foundations are ineffective due to its inability to withstand large overturning moments. Thus, multi-caisson foundations are preferred in deeper waters. Typically jacket or tripod foundations are preferred as multi-caisson foundation and these foundations are supported by either piles or suction caissons. Suction caissons are preferred due to the ease of installation and removal [1].

Based on the literature, it was understood that various kinds of research are being undertaken throughout the world to better understand the performance of suction caisson foundations. Two main components of suction caisson are researched widely, first being the installation behaviour, and second being the behaviour of caisson during repeated cyclic loading. This thesis seeks to gain further insight on the installation behaviour of the suction caisson. For this purpose, a suction installation apparatus was designed to be used in centrifuge. Various installation characteristics such as flow rate, soil profile has been studied in this thesis and detailed analysis is provided. Extraction tests of caisson were also done at a slow rate to determine the drained tensile capacity, which was used for determining tensile amplitudes in cyclic loading tests.

Tripod structures withstand load by 'push-pull' system, where the windward caisson is pulled out of the soil due to the cyclic environmental loads [2]. This movement is compensated by the push behaviour of the other two caissons. Thus, the tensile capacity of caissons plays an important role in the design of caissons in a tripod structure. Windward caisson of a tripod foundation was modelled in this thesis to study the behaviour of the caisson under cyclic loading in tension. Cyclic loading tests were done at 100g using the geo-centrifuge at Delft University of Technology. A series of tests was done for various cyclic loading characteristics such as the average load, frequency and soil profile. Settlement and stiffness response of the suction caisson were obtained for each scenario. A brief discussion of the results is made in this thesis report. Very high settlement was observed when one-way compressive load was applied on the caisson installed in layered sand. A test was also done to study the response of caisson to storm loading where very high tensile amplitudes were used. The results obtained from these tests show the complexity of the response under tensile loads. When the tensile amplitude was more than 50% of the

tensile capacity of the caisson, significant uplift of the caisson was witnessed along with a significant reduction in the stiffness of the soil.

Finally, Finite Element Modelling (FEM) was done using the geotechnical finite element software - Plaxis 2D to compare the cyclic loading results obtained from centrifuge modelling with FEM. It was observed that the initial settlement behaviour was captured well in plaxis. But after few cycles, no more accumulation of strain was witnessed in the centrifuge tests. However, plaxis failed to capture this behaviour and thus higher settlements were observed in FEM analysis.

This thesis can be used as a basis for the design of tripod foundations for OWT using suction caissons. The results obtained from this thesis reinforces previous studies and adds confidence in understanding the tensile behaviour of suction caissons.

Keywords: Suction Caisson, Offshore Wind energy, Sand layer, Cyclic loading, FEM.

Contents

List of Figures

List of Tables

List of Acronyms

OWT Offshore Wind Turbines

UNFCCC United Nations Framework Convention on Climate Change

CPT Cone Penetration Test

SPT Standard Penetration Test

DNV Det Norske Veritas

API American Petroleum Institute

JGS Japanese Geotechnical Society

MAP Manifold Absolute Pressure

LVDT Linear Variable Displacement Transducer

PIV Particle Image Velocimetry

FEM Finite Element Modelling

Chapter 1

Introduction

With the rise in global population and increasing demand for energy, non-renewable energy sources are being used at an alarming rate. This causes both serious depletion of energy and increase in pollution and global warming due to release of greenhouse gases. This was the reason to look for alternative energies which are cleaner and renewable. On 4^{th} of November, 2016, Paris agreement was signed by the 125 parties of United Nations Framework Convention on Climate Change (UNFCCC) to combat climate change [3]. This opened the door to the use of renewable energies such as solar, wind, and other clean energy sources. In Europe, due to less availability of solar energy in winters, wind energy is preferred. This led to a drastic increase in harvesting of wind energy as reported by Wind Europe [4]. Almost 65% of the renewable energy harvested in Europe in 2017 was wind energy as depicted in Figure 1.1.

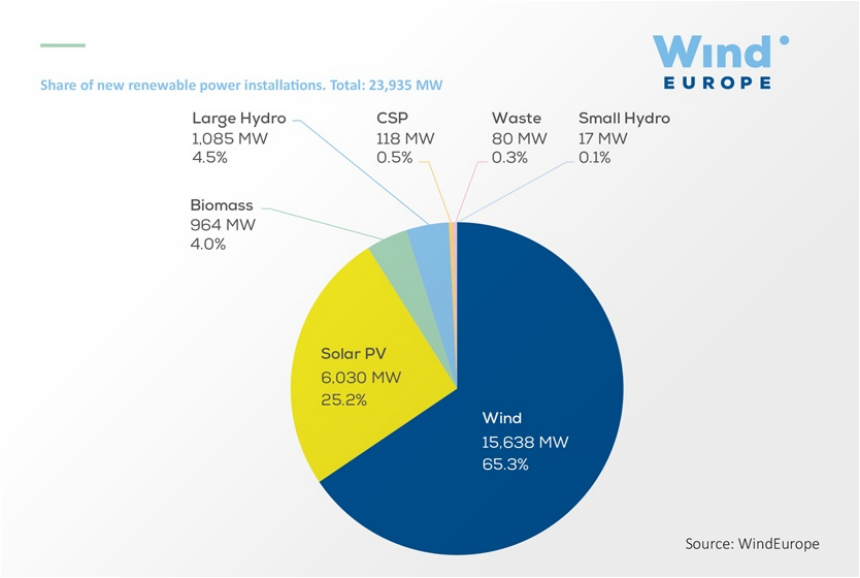

Figure 1.1: Proportion of renewable energy installations in Europe [4]

Traditionally wind energy was harvested using wind farms setup on the land. Due to the problem of noise that the turbines create and the inability to produce energy throughout

the year due to poor wind speed or physical blockages, installation of wind turbines in water bodies was proposed. Offshore wind farms have the advantage of uninterrupted wind supply and also bigger wind turbines with higher capacity can be built due to the availability of large areas [5].

1.1 Foundations for Offshore Wind Turbines (OWT)

Foundation design plays an vital role in installation of OWT onto the seabed. Loads acting on the superstructure is transferred to the soil using these substructures. To withstand these forces, a good design of foundations is necessary. Various types of foundations are present to support the offshore structures. Two widely used foundation types for OWT are discussed below:

1.1.1 Pile foundations

Due to the relatively shallow water depths, where OWTs are installed, very less overturning moments acts on the foundations. Thus, monopiles constitutes to almost 80% of the foundation used in OWTs and a schematic representation of monopile is shown in Figure 1.2 (a) [6]. Monopile foundations consist of long steel piles with a considerably big diameter. Monopiles are the desired foundation type for near shore and on shore applications. Dimensions of the pile depend on various parameters such as soil characteristics and loading characteristics. Typically, monopiles have a length over diameter (L/D) ratio of over 10. Installation of monopiles is done typically by using a hydraulic hammer or by the application of vibration drilling or by driving the pile into soil. Although monopiles constitute almost 80% of the offshore wind foundations, few problems are encountered on using monopiles and they are,

- As water depth increases, larger monopiles are required to overcome the large overturning moments. This is not economical.
- Higher installation costs due to the increase in time required for installation. Also, a lot of noise is created due to driving or hammering the pile.
- When boulders are present, this type of foundation is not suitable.

Multi pile foundations are typically used in Oil and Gas industry and thus are not discussed in this section.

1.1.2 Caisson foundations

Caissons are typically known as suction caissons or suction buckets. As the name suggests, caissons are cylindrical structures with a lid on top of them. Typical embedment (L/D) ratios of the caisson foundations are between 0.5 and 1. Caissons are installed by applying negative pressure i.e. removing water from the hole on the caisson lid and thus installation in very deep waters is also possible. Thus, caissons are widely used as anchors in deep waters as foundations for Oil and Gas platforms.

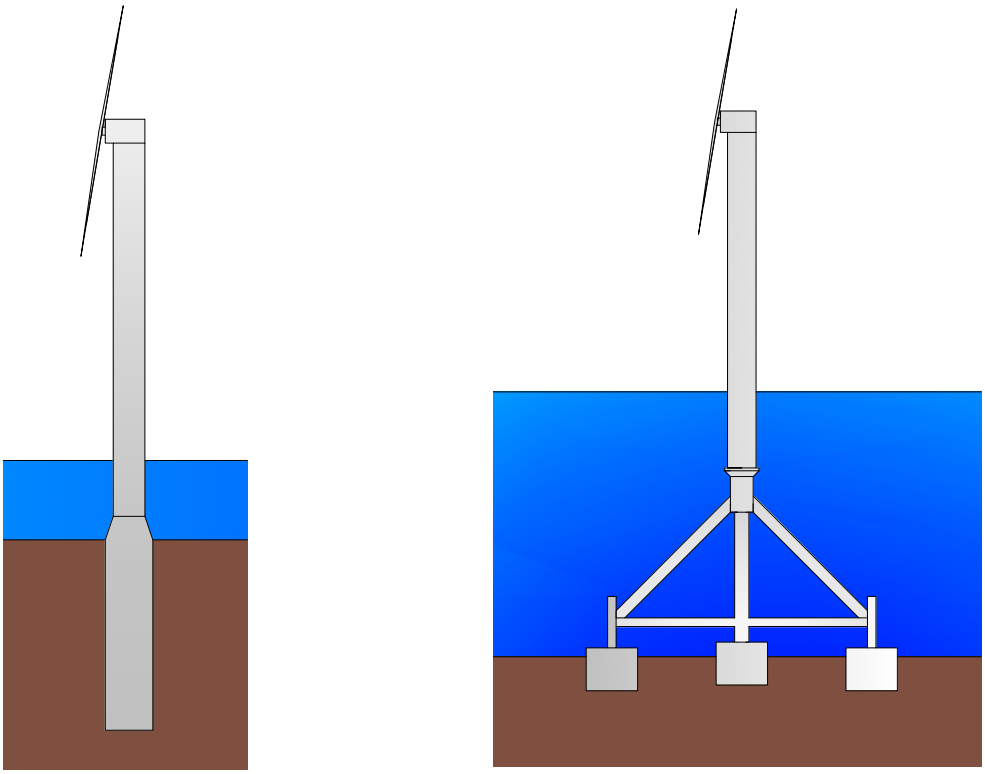

(a) (b)

Figure 1.2: Foundations for OWT a) Mono foundation b) Tripod foundation

The two types of caisson foundations discussed in this section are mono caisson and multi-caisson foundations. Use of suction to install mono caisson is very difficult due to the very high suction required for installation due to high skirt lengths. Nevertheless, suction caisson has a significant advantage over other foundation types due the ease of installation and decommission. In deeper waters, multi-caisson foundations are preferred due to their ability to balance significant overturning moments using the "push-pull" system. Tripod foundation with suction caisson is shown in Figure 1.2 (b). Advantage of using this type of foundation is cost driven. Few reasons why it has economic advantage are,

- Less requirement of steel for manufacturing the caisson due to smaller length.

- Lesser time required for installation due to the installation method.
- Possibility of reuse of foundation due to the possibility of extraction.

1.2 Problem definition

Design of the suction caisson involves several aspects such as installation, long term performance under cyclic loading and in some cases, extraction. Installation of the caisson involves two phases namely, self-weight penetration and suction assisted penetration. Various factors such as soil profile, soil characteristics play an important role in installation process. An understanding of all the factors involved in the installation process is necessary to avoid any failure during the process.

Long term behaviour of suction caisson under cyclic loading is analysed to study the stability of the foundation. As mentioned in the previous section, "push-pull" system is the primary phenomenon using which the overturning moments are resisted in a tripod foundation. Since the superstructure of OWT is not very heavy compared to an offshore oil rig, strict rotational limits of 0.25° is typically fixed for an OWT [7]. To this aspect, knowledge on the tensile capacity of the caisson is very important to make sure that rotational limit is not exceeded. Thus, the ability of a caisson to resist tensile loads in serviceability conditions is a dominant mechanism while designing a foundation.

In offshore conditions, soil profile is never homogeneous and varies spatially. But, owing to the difficulty in making a sample with layered soil profile, no research has been done on the response of suction caisson under cyclic loading in layered sand. Hence, in this thesis, a series of centrifuge tests has been done to study the effect of layered sand on the cyclic behaviour of suction caissons.

Upon decommissioning of the OWT after its design period, suction caisson can be reused in some other project. Thus, study on the extraction behaviour and validation of existing prediction model is vital to gain confidence in the models. In this thesis, a brief study on all the aspects of suction caisson will be discussed.

1.3 Aim of present research

As the title suggests, the main objective of this thesis is to study the *"behaviour of suction caisson subjected to vertical cyclic loading in tension"*. Based on this, the following research questions were formulated:

- How does the caisson installation response of caisson vary under various installation parameters?

- What would be the behaviour of caisson for various cyclic loading characteristics such as average load, frequency etc. under tensile loads?
- How would the cyclic behaviour of caisson vary when the soil profile is varied under various load types?

With this as basis, a suction installation apparatus was designed and assembled to install the caisson. Also, to determine the tensile amplitudes in cyclic loading, tensile capacity of the caisson was found using extraction tests. Cyclic loading tests were done in centrifuge for varying parameters such as cyclic amplitude, frequency and soil profile.

Also, based on previous research, it was understood that damage to the structure does not happen under serviceability loads. Thus, storm loads were also tested, where tensile amplitudes reached up to 60% of the tensile capacity.

Finally, validation of UBC sand model was done using Plaxis 2D to check the limitations and advantages of the model.

1.4 Outline of report

This report gives a detailed explanation of all the tests done in this thesis along with the theories behind them.

Chapter 1 gives an introduction to wind energy harvesting using offshore wind turbines. Foundations used for supporting OWTs are also discussed along with advantages and limitations. It is followed by the problem definition and aim of this thesis. This chapter also outlines the structure of the report.

Second chapter provides information about the two phases in suction caisson installation; 1. Self-weight penetration phase 2. Suction assisted penetration. A summary of all the existing prediction models to predict the suction required for penetration is provided. It is followed by a model made by Houlsby & Byrne to predict tensile capacity of suction caisson. Loads acting on an OWT as provided by DNV is also mentioned and response of caisson foundation to such type of cyclic loads is given. Finally, an overview of constitutive models used in Finite element analysis and correlations to obtain soil parameters is provided.

A detailed review about physical modelling is given in Chapter 3. Suction installation equipment was designed for installation of caisson. The motive behind selecting each component of the equipment is explained briefly. Dimensions of the suction caisson along with instrumentation is also provided. Also, information about the sands used, sample preparation method and soil profiles are mentioned. Then, details of installation, extraction and cyclic loading tests are provided.

Chapter 4 gives an insight into the finite element analysis done using Plaxis 2D in this thesis. In this chapter, discretization of model is done to provide the model geometry

along with the type of analysis undertaken. Problem is modelled to replicate the exact scenario in a centrifuge test. Also, soil and material properties used in the analysis are mentioned here. Then, boundary and initial conditions of the model are provided. Finally, loading scenarios or how the load is applied on the caisson is explained in the last part.

Fifth chapter presents the results obtained from all the tests carried out in this thesis by using the methodology mentioned in Chapter 3. Also, comparison of results obtained from the centrifuge tests and finite element analysis is given in this chapter. The last chapter of this report presents the main conclusions obtained from this thesis and provides recommendations for future researchers in order to gain more insight in this domain.

Chapter 2

Literature Review

This chapter provides the background and theory for installation of suction caissons followed by various prediction models for predicting the self-weight penetration depth and suction required for penetration. Also, model for predicting extraction resistance is also explained. Then, loads on OWTs is mentioned along with the response of soil to the loads. Finally, an overview is given about the constitutive models used in finite element modelling.

2.1 Installation Mechanism

Suction foundation installation is done in two phases. First phase involves self-weight penetration and second phase is suction assisted penetration.

Self-Weight penetration
In this phase, caisson/bucket is allowed to penetrate the sea bed under its own self-weight. Sufficient seal is needed for suction assisted penetration to take place and this seal is provided by the sand. If penetration is not enough, blowout of sand can take place. This can be explained as when suction is applied, seepage flow occurs, where water travels through the sand upwards, towards the suction valve. When insufficient seal is present, top layer of sand will be washed away by water and this hinders the whole installation process. Thus, more the self-weight penetration, better the installation process.

Suction assisted penetration
Pressure difference between inside and outside of the caisson is the predominant phenomenon which assists installation in sand during suction phase. This differential pressure on top of lid of the caisson applies a downward force on the foundation [9]. Water is pumped out through the opening in the caisson lid and this causes seepage flow to occur in the sand around the caisson tip as explained in Figure 2.1. Seepage flow is nothing but the flow of water through the soil from a low water gradient to high water gradient or as in this case, due to suction applied. This upward flow gradient reduces effective soil stress at caisson tip and along inner wall, thus reducing tip resistance and friction developed on internal caisson wall and hence, installation is possible even in dense sand [10].

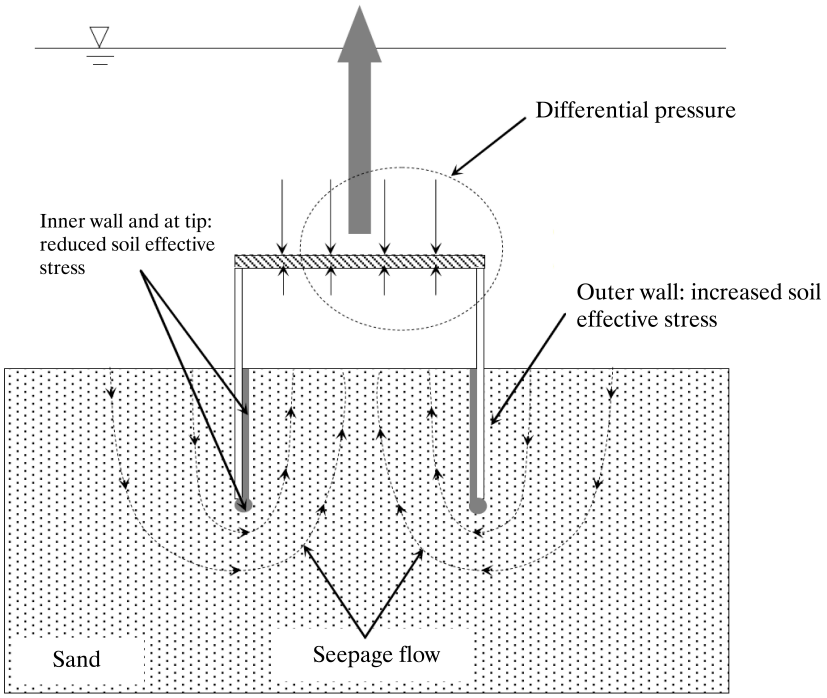

Figure 2.1: Illustration of seepage flow in sand (modified from M.N. Tran (2005) [8])

2.2 Prediction Models

Various prediction models have been developed for prediction of self-weight penetration depth and suction required for installation [11, 12]. Two types of prediction model exist based on Cone Penetration Test (CPT) approach and beta approach.

2.2.1 CPT Approach

CPT approach is followed by Det Norske Veritas (DNV) method and Senders and Randolph method. DNV method only describes the self-weight penetration phase while Senders and Randolph method uses cone penetration resistance to predict the self-weight penetration and suction required for penetration in dense sand. This method involves assessing the caisson resistance using cone penetration resistance and it is assumed that internal friction and tip resistance reduces linearly with increase in suction pressure. This is combined with flow model to determine water displaced by caisson, seepage flow into caisson and volume changes within pumping system [12]. This is a rather straight forward and accurate approach as very few numbers of parameters are needed as input when compared to Houlsby & Byrne prediction, which involves estimation of key input parameters such as N_q and K_0. No further details are provided on CPT approach as, in this study, beta approach will be used. This is due to the unavailability of CPT data for the sample prepared.

2.2.2 Beta Approach

Beta approach is followed by American Petroleum Institute (API) method and Houlsby & Byrne prediction. API does not specify a method to calculate installation resistance in suction caissons, but self-weight penetration depth can be calculated using design code provided for push-in resistance of piles in sand. Houlsby & Byrne method follows a more conventional approach in which the tip and internal frictional resistance are assumed to be in proportion to effective stress and modified by changes in effective stress due to seepage flow [13]. Detailed calculation for each phase for Houlsby & Byrne method is given in the following section:

Self-weight penetration
Resistance is calculated as the sum of friction on outside and inside of caisson and end bearing resistance. In this case, the caisson is modelled as a pile. Vertical equilibrium for the scenario is as follows:

$$V' = \frac{\gamma' h^2}{2}(Ktan\delta)_o(\pi D_o) + \frac{\gamma' h^2}{2}(Ktan\delta)_i(\pi D_i) + (\gamma' h N_q + 0.5t\gamma' N_\gamma)(\pi D t) \tag{2.1}$$

In the above equation, no account for stress enhancement in the soil near the pile due to frictional forces is taken. This leads to a non-conservative design where self-weight and suction predicted are less than required value.

Taking into account stress enhancement due to frictional forces of pile, it is assumed that friction distribution influences a zone of soil and it increases by a factor f_i and f_o inside and outside the caisson respectively. Zone at which vertical stress is enhanced by action of friction outside the caisson is assumed to be between diameters D_o and D_m where $D_m = mD_o$, where m is the multiple of diameter over which vertical stress is enhanced. It is also assumed that within this zone, stress is enhanced only vertically and not radially. If more realistic assumption is made, where $D_m = D_o + 2f_o z$ with f_o as constant,

$$Z_o = \frac{D_o[(1 + (2f_o z/D_o))^2 - 1]}{4(Ktan\delta)_o} \tag{2.2}$$

Similarly, zone at which vertical stress is enhanced by action of friction inside the caisson is assumed to be between D_i and D_n where $D_n = D_i - 2f_i z$ and this leads to,

$$Z_i = \frac{D_i[1 - (1 - (2f_i z/D_i))^2]}{4(Ktan\delta)_i} \tag{2.3}$$

Finally, end bearing resistance is calculated by assuming a triangular distribution at the tip and it is not symmetrical due to stress enhancement as shown in Figure 2.2. i.e stress on the outside of the caisson is not always equal to stress on the inside of the caisson. In this step, first $\sigma_{v_i'}$ and $\sigma_{v_o'}$ are calculated. If $\sigma_{v_i'} - \sigma_{v_o'} < \frac{2tN_\gamma}{N_q}$, then all the flow occurs inwards and end bearing resistance is as follows,

$$\sigma'_{end} = \sigma'_{vo} N_q + \gamma'(t - \frac{2x^2}{t} N_\gamma) \tag{2.4}$$

where,

$$x = \frac{t}{2} + \frac{(\sigma'_{vo} - \sigma'_{vi} N_q)}{4\gamma' N_q} \tag{2.5}$$

If $\sigma_{v'_i} - \sigma_{v'_o} \leq \frac{2tN_\gamma}{N_q}$. then all the flow occurs outwards and end bearing resistance is given as $x = 0$ and,

$$\sigma'_{end} = \sigma'_{vo} N_q + \gamma' t N_\gamma \tag{2.6}$$

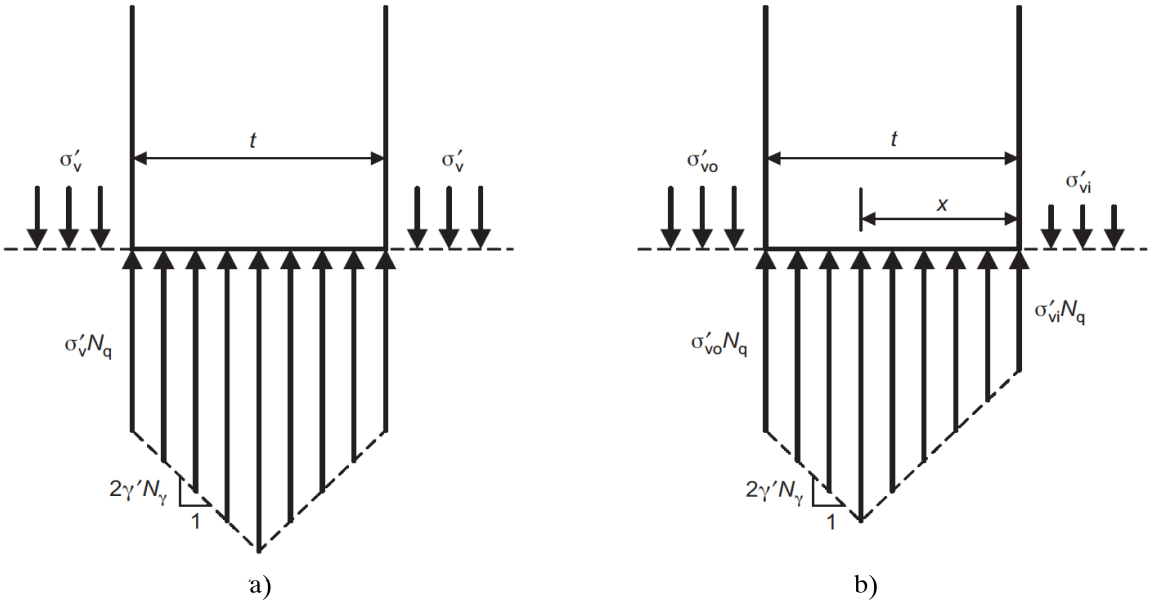

Figure 2.2: Stress distribution at caisson tip for a) $\sigma'_{vi} = \sigma'_{vo}$ b) $\sigma'_{vo} > \sigma'_{vi}$(Modified from Houlsby & Byrne (2005) [11])

When stress enhancement is accounted for, equation 2.1 becomes,

$$V' = \gamma' Z_0^2 [e^{(\frac{h}{Z_o})} - 1 - \frac{h}{Z_o}](Ktan\delta)_o(\pi D_o) + \gamma' Z_i^2 [e^{(\frac{h}{Z_i})} - 1 - \frac{h}{Z_i}](Ktan\delta)_i(\pi D_i) + \sigma'_{end}(\pi Dt) \tag{2.7}$$

Suction assisted penetration

If suction pressure, s is applied on top of the caisson with respect to outside water pressure, absolute pressure inside the caisson is $p_a + \gamma_w h_w - s$. If it is assumed that excess pressure

at tip of caisson is as, absolute pressure at caisson tip is given as $p_a + \gamma_w(h_w + h) - s$. This leads to an average downward hydraulic gradient of $\frac{as}{\gamma_w h}$ at outside the caisson and an upward gradient of $\frac{(1-a)s}{\gamma_w h}$ along the inside of the caisson. a is defined as pore pressure factor and since flow is restricted more on inside rather than outside the caisson, a is less than 0.5. a can be calculated using equation 2.8 and 2.9, which is an approximate fit for $k_f = 1$:

$$a_1 = c_0 - c_1[1 - exp(-\frac{h}{c_2 D})] \tag{2.8}$$

where, c_0, c_1 and c_3 are 0.45,0.36 and 0.48 respectively. These values are obtained by various finite element analysis. k_f is defined as the ratio of permeability of soil inside the caisson (k_i) to permeability of soil outside caisson (k_o). Since, more flow is assumed to occur inside caisson, k_i is more than k_o. a is affected by both depth of penetration and ratio k_f. This is given by following equation:

$$a = \frac{a_1 k_f}{(1 - a_1) + a_1} \tag{2.9}$$

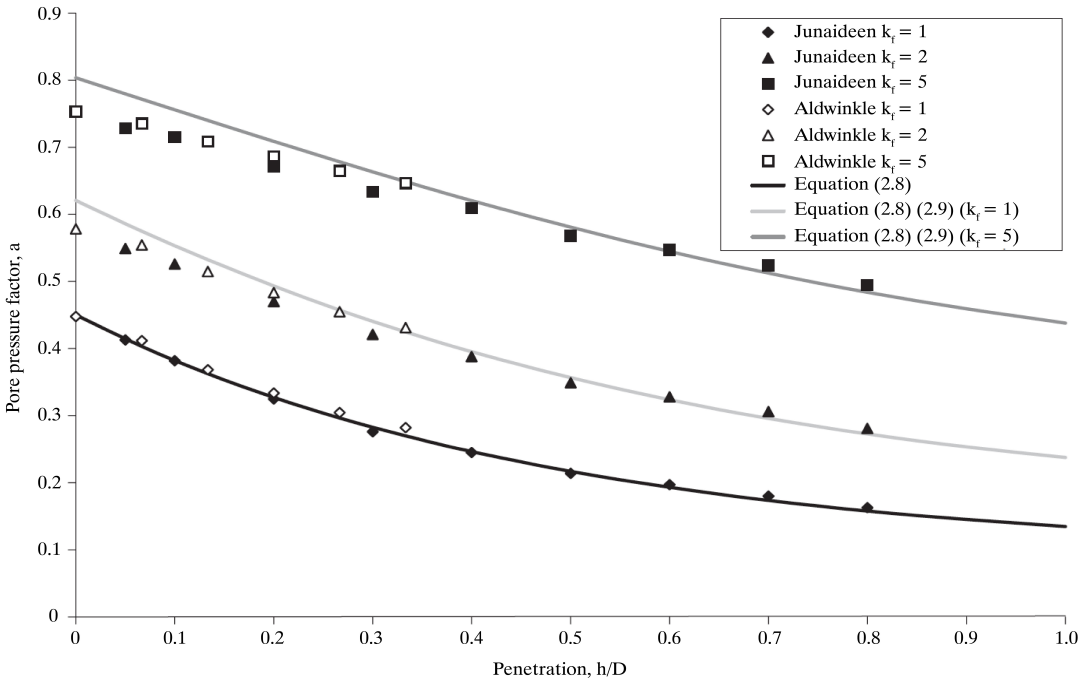

Figure 2.3: Variation of pore pressure factor "a" with penetration and "kf" (Modified from Houlsby & Byrne (2005) [11])

Figure 2.3 shows the graph for varying values of a with varying penetration and k_f.

Houlsby & Byrne assumed that distribution of pore pressure inside and outside the caisson is linear with depth. It is also assumed that failure occurs by soil moving inwards when internal vertical stress is reduced considerably. Solution for vertical stresses inside and outside the caisson are the same, except that γ' is replaced by $\gamma' + \frac{as}{h}$ for outside the caisson and $\gamma' - (1 - \frac{as}{h})$ inside the caisson. Thus equation 2.10 becomes:

$$\begin{aligned} V' + s\frac{\pi D_i^2}{4} = (\gamma' + \frac{as}{h})Z_o^2[e^{(\frac{h}{Z_o})} - 1 - \frac{h}{Z_o}](Ktan\delta)_o(\pi D_o) + \\ (\gamma' - \frac{(1-a)s}{h})Z_i^2[e^{(\frac{h}{Z_i})} - 1 - \frac{h}{Z_i}](Ktan\delta)_i(\pi D_i) + \\ [(\gamma' - \frac{(1-a)s}{h})Z_i[e^{(\frac{h}{Z_i})} - 1]N_q + \gamma' t N_\gamma](\pi D t) \end{aligned} \tag{2.10}$$

On solving this equation, suction required against penetration depth can be obtained.

2.3 Tensile capacity of suction caisson

Tensile capacity of pile plays an important role when a multi-caisson structure is designed for foundation in offshore conditions. This is due to the fact that; tripod structures in this case, counteract loads imposed on them by push-pull behaviour. This behaviour causes the windward caisson to experience tensile loads. Further information regarding push-pull system will be given in Section 2.5. Calculation of tensile capacities of caissons in two drainage conditions were provided by Houlsby & Byrne [13]. First is the drained condition and next is partially drained condition. Undrained capacity calculation is not provided due to the fact that in dense sand, cavitation occurs first due to accumulation of large pore pressures and also determination of undrained strength of sand is difficult.

Drained tensile capacity

When water is used in the centrifuge in a dense sand sample or when frequency is very low, drainage condition is considered as drained. And hence, no suction effect caused by the excess pore pressure on the lid of caisson is taken into account. Drained friction resistance is provided by the friction on the inside and outside of caisson wall. Tip resistance is neglected since it will be negligible. All the terms are calculated in the same way as self-weight installation prediction calculation. If no stress reduction is considered near the caisson due to frictional forces, tensile vertical load at penetration depth, h is given as,

$$V' = -\frac{\gamma' h^2}{2}(Ktan\delta)_o(\pi D_o) - \frac{\gamma' h^2}{2}(Ktan\delta)_i(\pi D_i) \tag{2.11}$$

A check should be always made that weight of soil inside the caisson is more than friction calculated inside the caisson. As in installation calculation, ignoring stress reduction proves

to be non-conservative. Hence, similar to installation calculation, including stress reduction leads to vertical tensile load as follows,

$$V' = \gamma' Z_0^2[e^{(\frac{h}{Z_o})} - 1 - \frac{h}{Z_o}](Ktan\delta)_o(\pi D_o) - \gamma' Z_i^2[e^{(\frac{h}{Z_i})} - 1 - \frac{h}{Z_i}](Ktan\delta)_i(\pi D_i) \quad (2.12)$$

where,
$Z_i = \frac{D_i}{(4Ktan\delta)_i}$ and $Z_o = \frac{D_i(m^2-1)}{(4Ktan\delta)_o}$;

Partially drained tensile capacity
On the other hand, when viscous fluid is used for centrifuge test or if tensile load is applied more rapidly, drainage condition is considered as partially drained and prediction model is changed accordingly. In this case, suction inside the lid of the caisson is taken into account. Similar to installation calculation for suction assisted installation, if suction pressure in the caisson is with respect to absolute pressure in the caisson, it is assumed that excess pressure at tip of caisson is as, absolute pressure at caisson tip is given as $p_a + \gamma_w(h_w + h) - s$. This leads to an average downward hydraulic gradient of $\frac{as}{\gamma_w h}$ on outside the caisson and an upward gradient of $\frac{(1-a)s}{\gamma_w h}$ along inside the caisson. Similar to installation calculation, along with difference in pressure between inside and outside the caisson, if assumption is made that m is constant and uniform stress is acting within the caisson, capacity of the caisson in tension is given as,

$$\begin{aligned} V' + s(\frac{\pi D_i^2}{4}) + as(\frac{\pi(D_o^2 - D_i^2)}{4}) = &-(\gamma' + \frac{as}{h})Z_o^2[e^{(\frac{h}{Z_o})} - 1 - \frac{h}{Z_o}](Ktan\delta)_o(\pi D_o) \\ &-(\gamma' - \frac{(1-a)s}{h})Z_i^2[e^{(\frac{h}{Z_i})} - 1 - \frac{h}{Z_i}](Ktan\delta)_i(\pi D_i) \end{aligned} \quad (2.13)$$

2.4 Loads on Offshore Wind Turbine

Loads acting on an offshore wind turbine structure plays an important role in design of the foundation as these loads are transferred to the substructure (foundation) embedded in the soil. Design of an OWT is dominantly based on the serviceability and not ultimate limit state as the design is typically dominated by stiffness of the foundation and performance under fatigue loading [9]. According to DNV (2014), loads acting on an OWT is classified into permanent loads, environmental loads, accidental loads and deformation loads [14]. In this research, accidental loads and deformation loads are not considered as they do not contribute to the cyclic behaviour of loading.

Permanent load
Self-weight of an OWT superstructure along with the substructure contributes to the permanent loads acting on the foundation. In this case, the substructure denotes the jacket

framework or the single slender column of OWT. Weight is calculated based on the amount of steel used in the construction of the structure. Self-weight of structure is not involved in cyclic behaviour. But, self-weight in combination with environmental loads contributes to the overturning moment which is cyclic in nature.

Environmental load

Cyclic loading on an OWT is triggered predominantly by environmental loads; primarily aerodynamic and hydrodynamic loads. Aerodynamic loads are caused by wind forces and contributes to the loads on support structure and wind turbine rotor. While load on support structure is directly related to wind speed varying with height and time, load on rotor depends on the angle of blades. Angle of blades is constantly changed using a pitch control system to obtain optimum power output and reduce the loads on blades [15]. Hydrodynamic loads are caused by the action of waves and currents on the substructure as explained in Figure 2.4. Intensity of wave and currents varies with space and time.

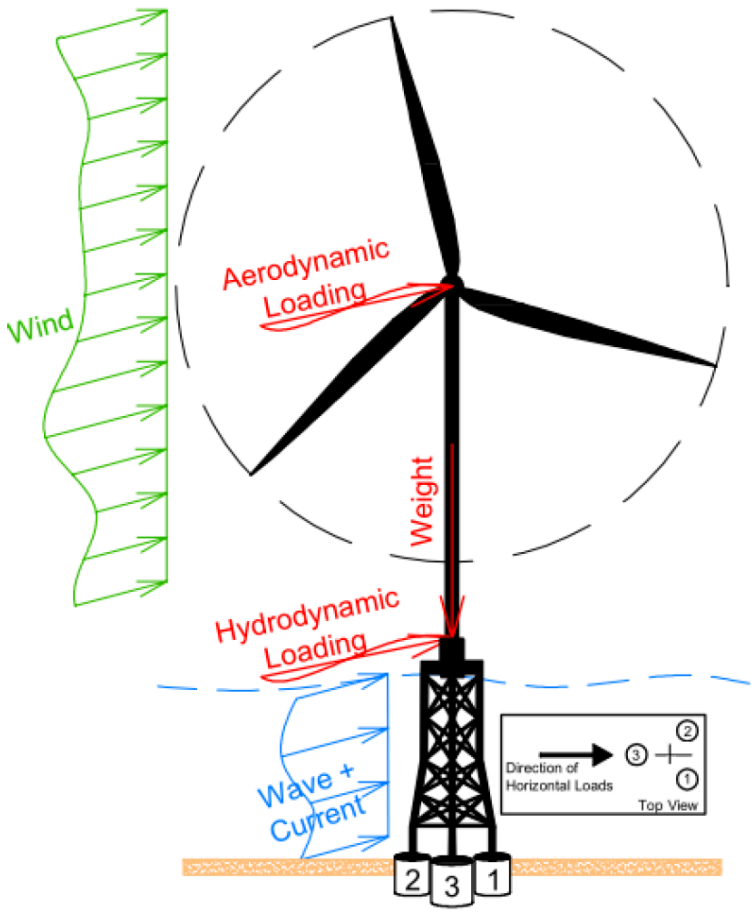

Figure 2.4: Loads acting on an OWT [15]

2.5 Foundation response to Cyclic loading

Based on previous experiences on offshore structures, it was found that when a mono-footing is used as foundation, self-weight of the structure along with environmental loads contributes to significant horizontal forces and moment loads on the foundation. Thus, significant concern on design is given to overturning moments for mono-footing design. In this thesis, since tripod foundation is analysed, overturning moments caused by horizontal loads are balanced by a "push-pull" motion of the foundation as mentioned by Byrne and Houlsby (2003) [2]. Push-pull is a system in which if predominant load is faced by a caisson/pile (i.e. windward caisson), this caisson gets pulled out of the soil and this movement is compensated by the other two caissons/piles (i.e. leeward caisson) in the system as shown in Figure 2.5. This pull behaviour contributes to tensile loading on the windward caisson.

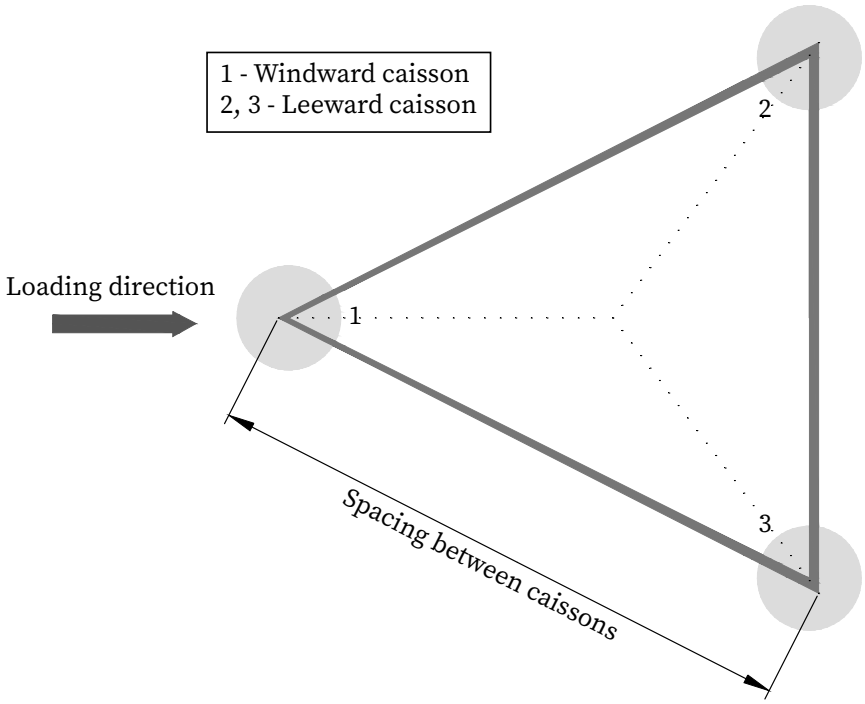

Figure 2.5: "Push-Pull" behaviour of the offshore tripod structure

In tripod foundations, horizontal loads are insignificant when compared to lateral capacity of the foundation [15]. Thus, design is dominated by vertical cyclic loads caused by the push-pull behaviour of the structure, with more importance given to the pull behaviour; i.e. tensile components [16]. To further solidify the statement, data provided by Dong E&P pvt ltd for C. Lupea's work has 47.5% of mean vertical loads in tension for windward caisson [15]. Based on literature, when tensile loading is applied to windward caisson, a softened response of the soil is witnessed immediately upon application of tension. When larger tensile loads are applied, the behaviour becomes stiffer and thus serviceability limits

play an important role in the design [17]. Also, due to the strict rotational limits of 0.25° imposed on OWT structures, it is important to study the settlement and stiffness behaviour of caisson under tensile loads and in particular, to study the role played by each characteristic of cyclic load (frequency, load amplitudes etc.) on the tensile behaviour of caissons.

2.6 Finite element modelling

Plaxis 2D is used to analyse the problem using finite element modelling and compare the results with centrifuge modelling. Various soil models are available in Plaxis and for cyclic loading applications, hypoplastic model and UBC sand model are preferred. In this research, UBC sand model was used as parameter determination of hypoplastic model is very complex and also from previous experiences, hypoplastic model did not match well with the centrifuge results. But for installation phase, it is not recommended to use UBC sand model as it gives unrealistic displacements. Hardening soil model is recommended for suction caisson installation phase. Detailed summaries of both the models are given in the following section.

2.6.1 Hardening soil model

Hardening soil model is a commonly used constitutive model to model both soft and stiff soils. Model is formulated using theory of plasticity and unlike the fixed yield surface in elastic perfectly-plastic model, yield surface of this model expands due to plastic straining. As the primary focus of this research is not hardening soil model, not much information is discussed. More details of this model can be found in Plaxis material models manual and an overview of parameter determination is given here.

Parameter determination for hardening soil model

Strength parameters of hardening soil model such as friction angle can be obtained from laboratory tests such as direct shear test. Stiffness parameters were obtained based on the correlations with relative density of the sand as follows,

$$E_{50}^{ref} = 60000RD/100 \tag{2.14}$$

$$E_{oed}^{ref} = 60000RD/100 \tag{2.15}$$

$$E_{ur}^{ref} = 180000RD/100 \tag{2.16}$$

Since stiffness of the soil model is stress-dependent, rate of stress dependency, m is negatively correlated with relative density as shown in Equation 2.17.

$$m = 0.7 - RD/320 \tag{2.17}$$

All these formulas were validated by R.B.J. Brinkgreve against triaxial test results [18].

2.6.2 UBC sand model

UBC sand is a 3D model developed for prediction of liquefaction behaviour in sands. Model is formulated using a classic plasticity theory with a hyperbolic strain hardening rule based on the original Duncan-Chang model. This model contains a 3D Mohr-Coulomb yield surface and a corresponding non-associated plastic potential function [19]. If σ_1 is the major stress and σ_3 is the minor stress, then yield surface and plastic potential are given as follows:

Yield surface:

$$f = \frac{1}{2}(\sigma_1 - \sigma_3) - (\frac{\sigma_1 + \sigma_3}{2} + c'cot\phi_p)sin\phi_{mob} \tag{2.18}$$

Plastic potential: Modified non-associated plastic potential function based on Drucker-Prager's criterion is used here [20].

$$g = q - M(p + c'cot\phi_p) \tag{2.19}$$

where,
$sin\phi_{mob} = \frac{(\sigma_1 - \sigma_3)}{(\sigma_1 + \sigma_3)}$, $M = \frac{6sin\psi_{mob}}{3 + sin\psi_{mob}}$ and $sin\psi_{mob} = sin\phi_{mob} - sin\phi_{cv}$;
ϕ_{mob} = Mobilised friction angle;
ϕ_{cv} = Constant volume friction angle;
ϕ_p = Peak friction angle;
ψ_{mob} = Mobilised dilatancy angle.

Hardening rule for UBC sand model follows a hyperbolic approach and it relates the increment of sine of mobilised friction angle to the plastic shear strain increments as shown in Equation 2.21. Non-linear rule controls the elastic behaviour within yield surface and are controlled by stress dependent modulus.

$$d\gamma^p = (\frac{1}{G^*})dsin\phi_{mob} \tag{2.20}$$

$$G^* = K_G^p(\frac{p'}{p_a})^{np}(1 - R_f\frac{sin\phi_{mob}}{sin\phi_p})^2 \tag{2.21}$$

where,
$d\gamma^p$ = Plastic shear strain increment;
K_G^p = Plastic shear modulus;
np = Plastic shear modulus exponent;
R_f = Failure ratio (0.9).

Hardening rule, formulated by Tsegaye (2010) [20] in UBC sand 3D model is as follows,

$$dsin\phi_{mob} = 1.5K_G^p(\frac{p}{P_a})^{np}\frac{P_a}{P_m}(1 - R_f\frac{sin\phi_{mob}}{sin\phi_p})^2 d\lambda \tag{2.22}$$

where, $d\lambda$ is the plastic strain increment multiplier.

Flow rule for UBC sand model is based on three observations namely, 1. At a constant ϕ_{cv} there is no plastic volumetric strain caused by plastic shear strains. 2. Stress ratio that lies below $sin\phi_{cv}$ exhibit contractive behaviour while those above exhibits dilative behaviour. 3. Difference between current stress ratio and stress ratio at $sin\phi_{cv}$ plays an important role on the amount of contraction or dilation. Flow rule is given as:

$$d\epsilon_v^p = (sin\phi_{mob} - sin\phi_{cv})d\gamma^p \tag{2.23}$$

where, $d\epsilon_v^p$ is the plastic volumetric strain increment.

Parameter determination for UBC sand model

UBC sand model has various stiffness, strength and advanced parameters. Stiffness parameters can be obtained either from curve fitting of Drained Triaxial tests or correlations with relative density or in situ tests such as Standard Penetration Test (SPT). Strength parameters such as ϕ_{cv} and c can be obtained from Consolidated Drained triaxial test or drained shear test. Advanced parameters such as R_f, f_{dens} and f_{Epost} can be obtained from curve fitting.

Stiffness parameters
Elastic shear modulus (K_G^e), elastic bulk modulus (K_B^e) and plastic shear modulus (K_G^p) can be obtained based on relative density as follows,

$$K_G^e \approx 1592RD^{(2/3)} \tag{2.24}$$

$$K_B^e \approx 0.7K_G^e \tag{2.25}$$

$$K_G^p \approx 16577RD^3 - 33623RD^2 + 20671RD - 2638 \tag{2.26}$$

Also, based on elastic bulk modulus and elastic shear modulus, poissons ratio (ν') can be obtained based on following relation,

$$\frac{K_B^e}{K_G^e} = \frac{2(1+\nu')}{3(1-2\nu')} \tag{2.27}$$

Strength parameters
Based on ϕ_{cv} obtained from direct shear test, ϕ_p can be obtained using correlation with SPT data, $(N1)_{60}$. Since $(N1)_{60}$ is not available based on in-situ testing, it can be obtained based on correlation with relative density as follows,

$$(N1)_{60} = \frac{RD^2}{15^2} \tag{2.28}$$

Where relative density is in percentage. ϕ_p can be found using equation 2.29 as follows,

$$\phi_p \approx \phi_{cv} + \frac{(N1)_{60}}{10} + max(0; \frac{(N1)_{60} - 15}{5}) \tag{2.29}$$

Advanced parameters
Failure ratio, R_f has a default value of 0.9, but it can also be obtained from SPT value $(N1)_{60}$ as follows,

$$R_f \approx 1.1((N1)_{60})^{-0.15} < 0.99 \tag{2.30}$$

Densification factor, f_{dens} is a multiplier that controls the scaling of plastic shear modulus factor during secondary loading. Above 1, plastic shear modulus becomes high and stiffer and below 1, plastic shear modulus becomes lower and softer. f_{Epost} is a fitting parameter to adjust post liquefaction behaviour and it has value of 0.2-1.

2.7 Conclusion

From literature review, various aspects of suction caisson foundation were understood. From installation to extraction and cyclic loading, various researches have been done. With this knowledge, various prediction models have been developed for installation and extraction behaviour by leading research groups in the world. Of all the methods available for prediction, Houlsby & Byrne method is believed to be better suited when no CPT data is available.

Due to the complexity in the response of foundation to cyclic loading, tests were done on the various characteristics of cyclic loading, such as frequency, amplitude, average load etc. All these characteristics had a significant impact on the accumulation of strain and the stiffness response of the soil. But not many centrifuge tests were done to study the response of model to tensile loading in prototype conditions. In offshore conditions, soil profile is rarely homogeneous throughout the depth of foundation and usually consists of multiple layers. But no test has ever been done to study the behaviour of layered sand in response to vertical cyclic loading. Possible negative effects of cyclic loading should govern the design of foundation in sand. Based on this aspect, centrifuge tests were done in this

research to study the effect of load characteristics on stiffness and displacement response of caisson in both homogeneous and layered sand. Also, installation and extraction tests were done (Chapter 3).

Furthermore, a review of models available to simulate a cyclic loading problem in Plaxis were discussed. With respect to simplicity in obtaining model parameters and obtaining better results, UBC sand model was decided to be used to model the soil behaviour subjected to vertical cyclic loading in tension (Chapter 4).

Chapter 3

Physical Modelling

To study the behaviour of suction caisson, experiments should be done on a caisson installed by applying suction. Installation by applying suction causes changes in soil density and permeability when compared to jacked or driven installation, where no such changes are witnessed. To capture this behaviour, a suction caisson installation apparatus was designed to install the caisson as explained in the previous chapter.

All the dimensions of the apparatus provided in this chapter are based on a model scale. This chapter describes the experimental details of tests carried out in the centrifuge. A model suction caisson, scaled down from prototype was used for installation, extraction and cyclic loading tests. Also, a detailed review of the equipment design, experimental procedure and sample preparation is presented. Finally, an overview of the centrifuge tests is provided.

3.1 Geo-centrifuge

In most experimental studies, performing an ideal full-scale test is difficult due to the constraints of cost and time. It is also not possible to replicate a real scale scenario in a laboratory test as soil stresses developed in sample lab models are very less when compared to real scale. In order to study the prototype soil-structure interaction in a laboratory, centrifuge tests were developed. Centrifuge tests are less time consuming and cost significantly less when compared to full scale tests. Soil stresses in a prototype scenario can be replicated in the model inside the centrifuge.

In order to extrapolate results obtained in model tests to prototype scale, various scaling laws have been developed. Scaling laws for few of the parameters used in this thesis are mentioned in Table 3.1 and were obtained from the book "Centrifuge Modelling for Civil Engineers" [21].

Tests conducted as a part of this thesis have been carried out in the Geo-Centrifuge at the Delft University of Technology. It is a beam type centrifuge with two swinging carriers on either side of a rotating arm. A short summary of the specifications of the centrifuge is given below,

- The maximum working space of the carrier is 400x400x500 mm. This gives a prototype dimension of 40x40x50 m at an acceleration level of 100g.
- Distance from the center of the centrifuge to the base of swinging carrier during rotation is 1.2 m.
- Samples with a weight of 30 Kgf can be tested up to acceleration levels of 160g.

Parameter	Model/Prototype
Length	1/N
Area	$1/N^2$
Volume	$1/N^3$
Force	$1/N^2$
Stress/Pressure	1
Relative density	1
Time	1/N
Frequency	N

Table 3.1: Centrifuge scaling laws for parameters used in this thesis

3.2 Apparatus

In this section, various components used in the suction installation apparatus and the motive behind selecting each component is explained.

3.2.1 Strong Box

A square strong box with a dimension of 305 mm was used in this thesis. Internal dimensions of the strong box were 295x295x170 mm as shown in Figure 3.1 . It was made of aluminium and mounted on a 10 mm thick aluminium plate. In order to nullify any boundary effect, lateral boundary had to be at least 4 times the radius of the caisson from the center of the caisson [8]. Also, since installation was done in sand, the predominant mechanism for suction installation to occur was seepage flow. In order to have unrestricted seepage flow, bottom boundary had to be at least 1.6 times the skirt length [8]. In this thesis, dimension of the strong box was based on the maximum size of the apparatus that can be placed in the carriers of the centrifuge and the caissons were designed accordingly to nullify boundary conditions.

If a free board height of 15 mm is provided, maximum height of the caisson that can be tested in this strong box without any hindrance to seepage flow at bottom is 59.5 mm.

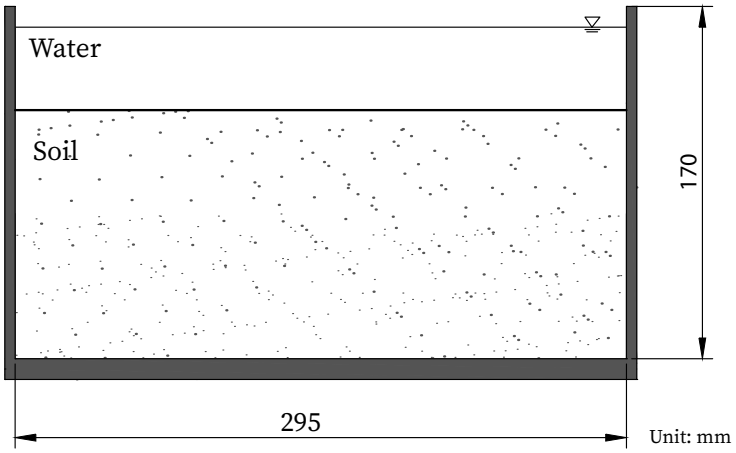

Figure 3.1: Schematics of the strong box

Also, with respect to the lateral boundary, maximum diameter of the caisson that can be tested is 80 mm.

Pore fluid used in this thesis was de-aired water. A viscous fluid could not be used as pore fluid due to two reasons: 1. Preparation of dense soil samples using a fluid of certain viscosity cannot be done using normal sample preparation methods such as wet pluviation or using vacuum chamber. 2. Fluidisation setup, generally used for preparation of soil sample with viscous fluid, was not included in the strong box due to time constraint.

3.2.2 Suction caisson

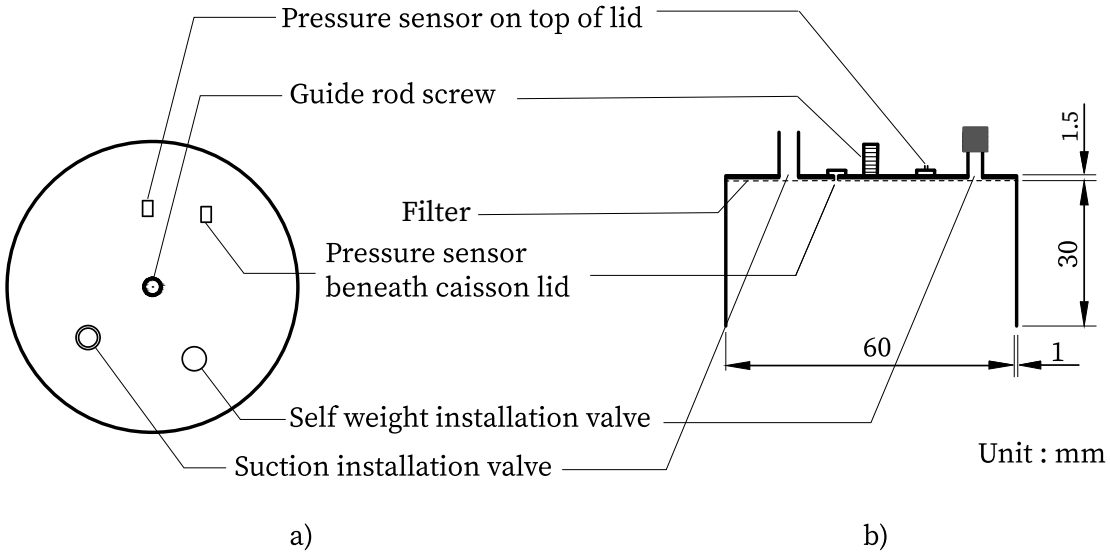

Figure 3.2: Schematics of instrumented suction caisson a) Plan view b) Side view

In this thesis, tests were designed to simulate a windward caisson of a tripod foundation which supports an OWT. It has to be noted that the windward caisson varies with respect to loading direction. A suction caisson usually has a typical embedment (L/D) ratio between 0.5 and 1. To study the worse- case scenario, a suction caisson with a L/D ratio of 0.5 was designed. With that embedment ratio, diameter of the caisson was chosen as 60 mm and skirt length was chosen as 30 mm in the model scale. As tests in centrifuge were done at 100 times the gravitational field (g), this attributes to a prototype diameter of 6 m and skirt length of 3 m. The caisson skirt and lid had a thickness of 1 mm and this translates to 100 mm in prototype. A fine filter with a thickness of 0.5 mm was placed beneath the caisson lid to avoid damage to the sensors and also to prevent sand outflow during suction application. Top lid had three holes/openings in it; for the pressure sensor, for the suction installation valve and for the self-weight installation valve. A schematic of the model caisson is shown in Figure 3.2.

3.2.3 Pump and solenoid valve

In this section, electrical parts used in the installation process are discussed. Two methods used for installation of the caisson are discussed in detail in Section 3.2.7. For the first method, in order to apply necessary negative pressure or suction for installation of the suction caisson, an external gear wheel pump was used. External gear pump is a positive displacement pump composed of a casing with two meshing gears with external teeth to facilitate flow [22]. In order to supply power to the pump, a 12 V rechargeable battery was attached to the centrifuge stem.

In the second method, a pneumatic solenoid valve was used to control the installation process during gravity flow. It is an electro-mechanical valve in which the solenoid (electromagnet) uses an electric current to generate magnetic field and this field exerts a force on the plunger, which is pulled towards the centre of the coil to open the orifice. It is a spring valve controlled using the control computer. Flow was achieved using the head difference between the water in strong box and the reservoir.

3.2.4 Pressure transducers

Manifold Absolute Pressure (MAP) sensors used in this study were manufactured by NXP semiconductors. They have a better accuracy than many other sensors in the market against temperatures generated inside the centrifuge chamber and have a range of up to 250 kPa. All the sensors were calibrated using the centrifuge control software.

Three MAP sensors were used in the caisson setup. The first sensor, P1 (refer Figure 3.5), was glued to the bottom of the reservoir and was calibrated against the depth of water. This was used to measure the flow rate during installation process. The second sensor, P2, was glued to the top of the caisson. It was used to measure the hydro static pressure acting on top of the caisson. The third sensor, P3, was fixed to the bottom of

the caisson lid and was used to measure the pore pressure developed inside the caisson during cyclic loading. Also, difference between the pressure reading obtained from P3 and P2 sensors gave the suction acquired during installation. Both P2 and P3 sensors were calibrated against hydro static pressure using the unit weight of water i.e., 9.8 kN/m^3. All the sensors were covered using epoxy glue on the outer surface as the caisson was immersed inside water for a considerable period of time.

3.2.5 Reservoir

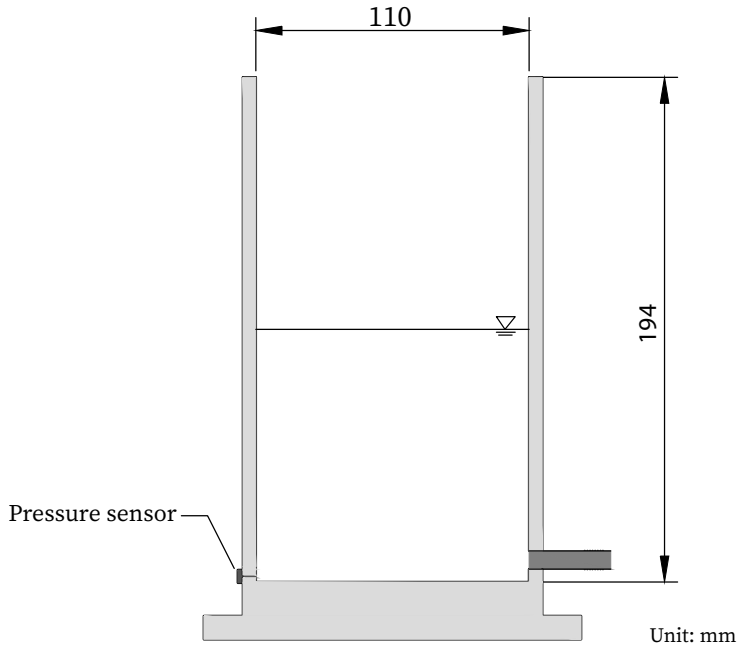

Figure 3.3: Schematics of the reservoir

Cylindrical reservoir was used to collect the de-aired water pumped out of the suction caisson during installation and also to measure flow rate during installation process. A 5 mm thick plastic cylinder was used to withstand the high pressures created in the centrifuge. Internal diameter and depth of the cylinder were 110 mm and 194 mm respectively as shown in Figure 3.3. MAP sensor was glued to the lowest point at the bottom of the reservoir to measure the water depth. By knowing the depth of water, density of fluid and area of cylinder, flow rate can be calculated. For installation using pump, reservoir was kept empty before the test and 5 mm diameter pipes were used to facilitate the connection with the pump, reservoir and caisson.

For installation using gravity flow, 7 mm diameter pipes were used in order to obtain an increased flow rate. Water level was kept just above the orifice inlet in the reservoir in order to avoid formation of air bubbles inside the pipe and also to achieve a maximum head difference between strong box and reservoir. Also, all the pipe connections were kept

below the water level in strong box in order to make sure no air bubbles were present in the pipe. Larger pipes could not be used as connection with suction installation valve in the caisson could not be made air tight.

3.2.6 Guide rod and loading actuator

A guiding system was used to make sure that the suction caisson did not tilt during installation. The guiding system comprised of a guide rod of 4 mm diameter and two guide screws. One end of the rod was screwed to the suction caisson and the other end was fixed to a Linear Variable Displacement Transducer (LVDT) to measure the vertical displacement of the caisson. To eliminate any movement in the lateral direction, the guide rod was made to pass through a hole in the actuator. During the installation phase, the rod was let to move freely with respect to the caisson movement in the vertical direction in order to nullify any resistance/friction during installation process. Illustration of the setup is provided in Figure 3.4.

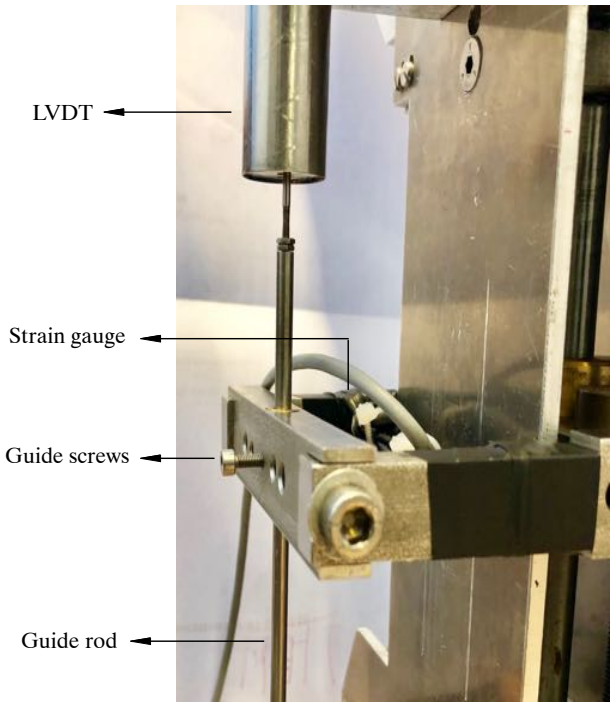

Figure 3.4: Illustration of the guiding system

Two guide screws were placed on either side of the hole in the loading actuator. The guide rod was fixed to the loading actuator by tightening the guide screws for self-weight installation phase, cyclic loading and extraction tests. The load applied was measured using strain gauges attached on the cantilever extension of the loading frame. A loading actuator is a computer-controlled load application device, using which both vertical and horizontal loads can be applied when the centrifuge is spinning.

3.2.7 Suction caisson installation setup

Two methods were used for installation of the suction caisson. Firstly, gravity flow method was used to create the suction required for installation. This was achieved using the head difference between the water in the strong box and in the reservoir. Ideally the head difference was kept at 15 cm by maintaining the water level in strong box at 16 cm and at 1 cm in the reservoir. To achieve flow, no air bubbles should be present inside the pipe. Presence of air bubbles can cause cavitation inside the pipe and thus can hinder the flow. A pneumatic solenoid valve was used to control the installation as mentioned in section 3.2.3. Figure 3.5 shows the complete setup for gravity flow.

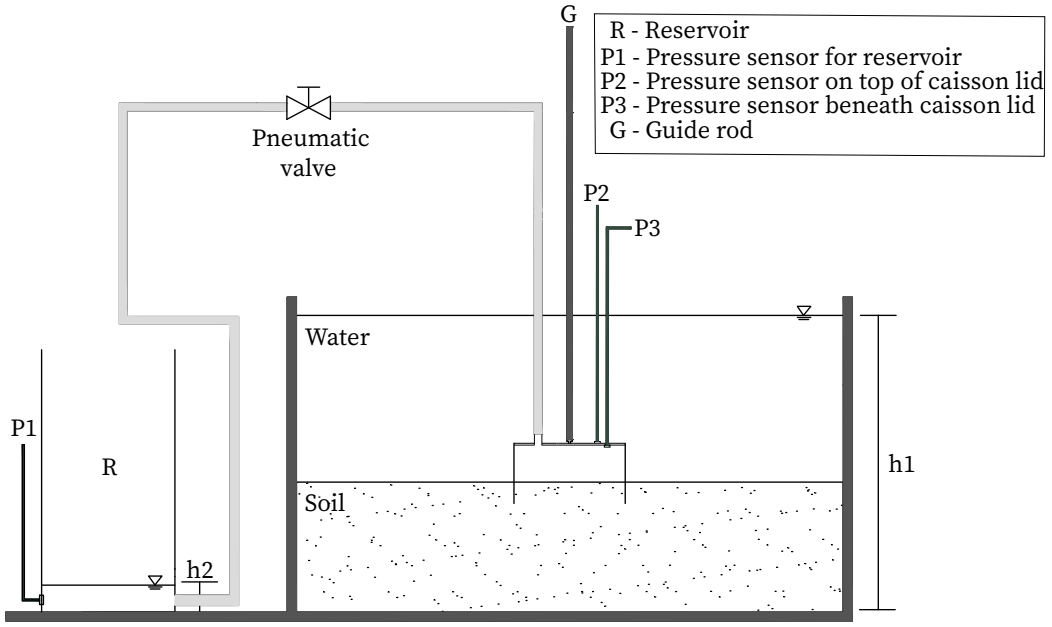

Figure 3.5: Setup for installation using the gravity flow

Secondly, as shown in Figure 3.6 and discussed in Section 3.2.3, a gear wheel pump was used to apply the necessary suction. To control the flow rate, a needle valve which was operated manually was used.

3.3 Soil description

Two different types of soils were used in this thesis, namely; fine silica sand and a very fine silica sand. Both the sands were provided by Sibelco (NL).

Fine silica sand is denoted as silica sand in this thesis and the grain particles were sub-rounded with a specific gravity of 2.65. Maximum and minimum grain sizes were 0.5 mm and 0.2 mm respectively. It was used to prepare the homogeneous soil layer. Few basic lab tests were done to characterise the sand. Minimum and maximum void ratios of the sand

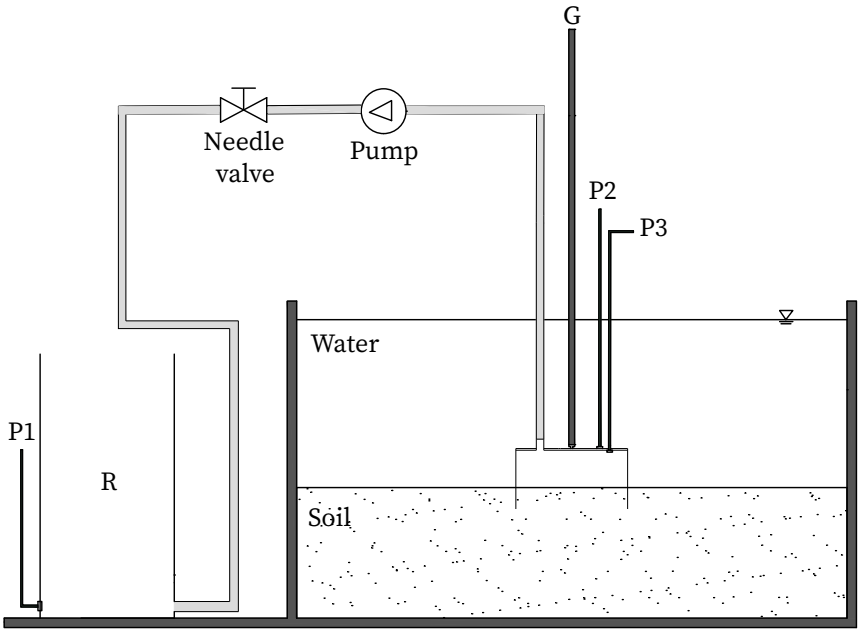

Figure 3.6: Setup for installation using the pump

were found using Japanese Geotechnical Society (JGS) method. Strength properties of the sand were obtained using direct shear test. The samples for direct shear test were prepared in a similar density to that of the centrifuge tests. Further details about the laboratory tests and sand properties are provided in Appendix A.

Geba sand denotes the very fine silica sand. It was used to simulate a less permeable layer on top of the homogeneous silica sand. Grain particles of geba sand were also sub-rounded with a roundness coefficient of 0.77 ±0.01 [23]. Specific gravity of this sand was 2.67 and it was composed of about 8% of silt sized particles with 84% of the sand passing through a 100 mm sieve. Table 3.2 summarises the mechanical properties of both the sands.

Parameter	Silica sand	Geba sand
Maximum void ratio	0.86	1.07
Minimum void ratio	0.625	0.64
D_{50}	0.390 mm	0.11 mm
Friction angle (ϕ_{cv})	34.1°	36°
Cohesion	0 kPa	0 kPa
Permeability	8.41E-4 m/sec	4.2E-5 m/sec

Table 3.2: Properties of silica and geba sand

3.4 Sample preparation

Various methods are suggested in the literature for preparation of saturated soil samples. Key factors involved in selection of the sample preparation method are uniformity of sample, preparation time and control over density of the sample. Due to the difference in the properties of sands used in this thesis, slightly varying methods were used for preparation of the homogeneous sand sample and the layered sand sample. Both methods were adapted based on literature provided by M.N. Tran (2005) [8].

Homogeneous sand sample
For preparation of homogeneous sand sample, the strong box was first filled with de-aired water and was placed on a vibrating table. Dry silica sand was then pluviated into the strong box at a very slow pace using a pluviation bucket. Continuous vibration was applied during the pluviation process. Once the soil height reached 20 mm, additional vibration was applied by dropping the strong box 5 times from a height of 50 mm to further densify the sample. Process was repeated till the desired sample height of 70 mm was achieved. Then, vibration was continued for a period of 15 minutes. This resulted in a uniform sample with a relative density of about 75%. Further control over density can be achieved by changing the fall height, size of openings and number of openings in pluviation bucket. Weight of the sample was calculated at three phases to determine the relative density; firstly, empty weight of the strong box; secondly, after water is filled in the strong box and finally at the end of the sample preparation process. Typical cross section of the prepared homogeneous sample is presented in Figure 3.7.

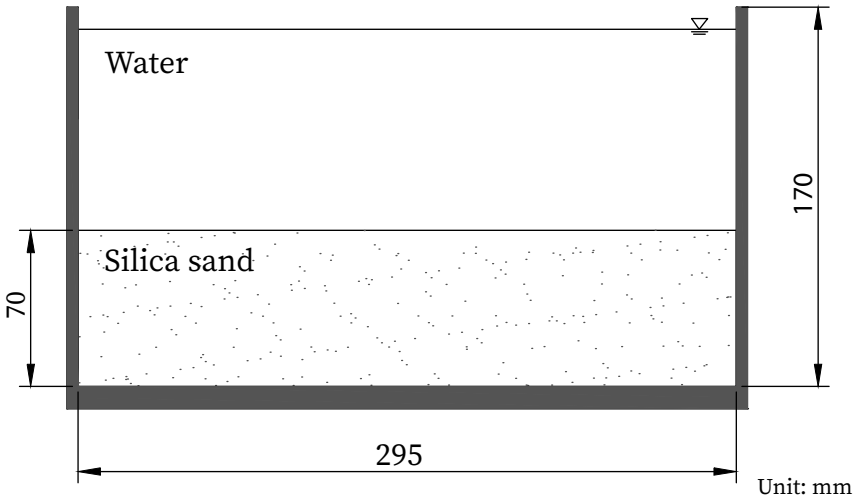

Figure 3.7: Schematics of the homogeneous sand profile

Layered sand sample
For layered sand, bottom silica sand layer was prepared to a depth of 60 mm using the method mentioned above. Geba sand was then added on top of the dense silica sand without any vibration. Sufficient time was given for the silt fines to settle and then vibration

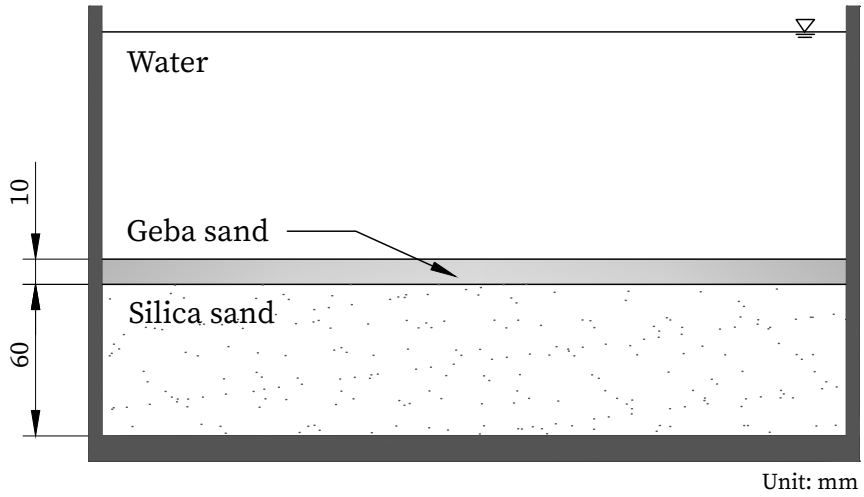

Figure 3.8: Schematics of the layered sand profile

was applied. Short vibration period was used for approximately 5 minutes. After vibration, depth of less permeable geba sand layer was approximately 10 mm as shown in Figure 3.8 and this gave a relative density of 55%. Longer vibration, or vibration during pluviation of geba sand caused the sands at the interface to mix.

3.5 Test procedure

Procedures for the installation of suction caisson, extraction and cyclic loading are summarised in this section.

3.5.1 Installation of suction caisson

All the installation tests in this thesis were done at 1g. As mentioned in Section 3.2.7, installation of the caisson was done using two mechanisms differing in the way by which the suction was applied. Procedure for installation using these two methods are explained below.

Installation using pump

- Saturated sample prepared in the strong box was placed in the centrifuge carrier which was fitted with a loading actuator.
- Caisson was slowly and completely submerged into the de-aired water in a diagonal manner to get rid of any air bubbles underneath the caisson lid. The self-weight installation valve open during this process. Caisson was then fixed to the guide rod before gently placing it on the soil surface.

- Caisson was then allowed to penetrate the soil under its own self-weight. Once no movement of the caisson was witnessed, guiding screws were tightened to the loading actuator.
- Using the loading actuator, self-weight installation was done to a depth of 10 mm using the actuator with a displacement rate of 0.05 mm/sec. Once self-weight installation was done, self-weight penetration valve was sealed, and guide screws were released.
- Suction assisted penetration was conducted by applying suction using a pump up until the caisson lid came in contact with soil surface.

Installation using gravity flow
Till the self-weight installation phase, the same steps as followed for installation using pumps were followed. Suction assisted installation was then performed by releasing the solenoid valve and letting the water to flow from strong box to reservoir. Valve was closed when no more penetration of the caisson was witnessed. In this thesis, initial flow rate attained using gravity flow was 25.17 ml/sec. Flow rate decreased as the head difference decreased. Overall flow rate of 7.52 ml/sec was attained.

3.5.2 Cyclic loading

Once installation was done, the centrifuge was accelerated to 100g and cyclic loading tests were done in a load-controlled manner using the loading actuator. Number of cycles, compressive and tensile amplitudes were specified in the centrifuge control computer and frequency was controlled by changing the loading rate. The compressive amplitude was fixed at 50N (model scale) in all of the tests except storm loading test. The idea behind this is explained in Section 3.6.2. Since loading was done in load-controlled manner, the loading rate had to be changed for each test with different amplitudes to maintain the same frequency. Table 3.3 gives an overview of the loading rates used along with the corresponding loading amplitudes. Also due to a very slight delay in the feedback loop, it was noticed that load amplitude and frequency varied for a requested cycle within each test. If higher loading rates were used, difficulty in control over the load amplitude and frequency occurred. Thus, a maximum frequency of 0.028 Hz (model scale) was used in this research. In almost all of the tests, frequency of the load applied was maintained at 0.028 Hz. In one test, loading at a lower frequency of 0.014 Hz (model scale) was tested.

3.5.3 Extraction of suction caisson

Once installation or cyclic loading test was performed, extraction of the caisson was done at 100g. With the caisson attached to the loading actuator using guide screws, extraction

Compressive load (N)	Tensile load (N)	Frequency (Hz)	Loading rate (mm/sec)
50	0	0.028	0.0155
50	-50	0.028	0.025
50	-50	0.014	0.0155
50	-70	0.028	0.033
50	-85	0.028	0.0375
50	-110	0.028	0.041

Table 3.3: Overview of loading rate corresponding to a loading amplitude and frequency (model scale)

was done by pulling the suction caisson at a slow rate of 0.001 mm/sec to facilitate drained condition. Extraction tests were stopped when the tensile capacity value reached a plateau to save time.

3.6 Overview of tests

An overview of all the tests done in this thesis is presented in this section. Tests done include installation tests at laboratory conditions (1g), and extraction and cyclic loading tests performed at 100g. All the tests were done in the strong box and samples were saturated with de-aired water. Few tests were done initially to test the relationship between the loading rate and frequency for different load amplitudes. They are not reported in this report.

3.6.1 Installation & extraction

Installation was done at laboratory conditions and during installation, vertical displacement of the caisson, pressures inside and outside the caisson, and flow rate were recorded. Suction required for installation was applied either using a discharge pump or with the aid of gravity flow. Installation using pump was done at slow and fast flow rates to study the effect of flow rate on installation. 34.8 ml/sec denotes the fast flow rate obtained and it was achieved by fully opening the needle valve. A slow rate of 20.7 ml/sec was achieved by closing the pipe using the needle valve as much as possible without completely stopping the flow. Further lower rates could not be achieved due to the higher stiffness of the pipe. Installation done using gravity flow did not have a constant flow rate as pressure inside the pipe decreased with decreasing head difference. Tests were also done by varying the soil profile to study the effect of less permeable sand layer on the installation process. Details of each test scenario are mentioned in Table 3.4.

Test name	Soil type	Test type	Flow rate (ml/sec)
IT-1	Homogeneous	Pump	34.8
IT-2	Homogeneous	Pump	20.7
IT-3	Homogeneous	Gravity flow	7.52 (Varied)
IT-4	Layered	Pump	34.8

Table 3.4: Overview of installation tests

As mentioned in Section 3.5.3, extraction was done after all of the tests at 0.001 mm/sec to determine the drained tensile capacity of the caisson.

3.6.2 Cyclic loading

Cyclic loading tests were done at an acceleration level of 100g after installation of the caisson was done at laboratory conditions. During cyclic loading, load applied, vertical displacement of the caisson and pressures inside and outside the caisson were recorded. As shown in Figure 3.9, maximum amplitude in compression was fixed based on the buckling capacity of the guide rod. Since main aim of this thesis is to study the tensile response of the caisson, higher compressive loads were not used. This also helped in avoiding any bending of the guide rod during loading, which would have caused some discrepancies in the vertical displacement measured.

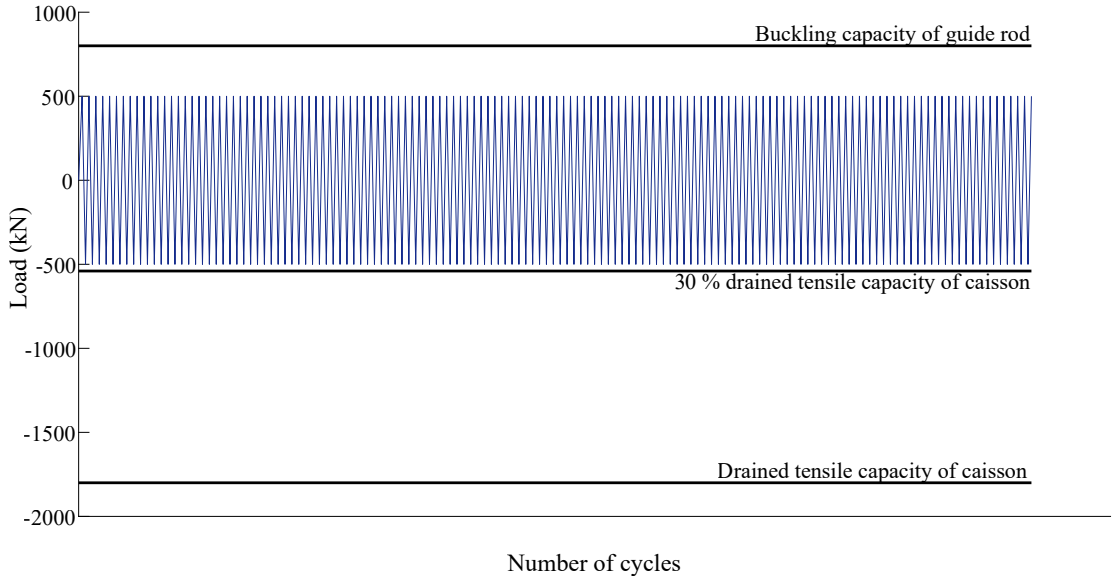

Figure 3.9: Basis for determining the compressive and tensile amplitudes (prototype scale)

Test name	Soil profile	Average load (kN)	Max. compressive load (kN)	Max. tensile load (kN)	Frequency (Hz)
CL-1	Homogeneous	250	500	0	0.00028
CL-2	Homogeneous	0	500	-500	0.00028
CL-3	Homogeneous	Storm	Varied	Varied	0.00028
CL-4	Homogeneous	0	500	-500	0.00014
CL-5	Layered	250	500	0	0.00028
CL-6	Layered	0	500	-500	0.00028

Table 3.5: Overview of cyclic loading tests (prototype scale)

Amplitudes in tension were determined based on the drained tensile capacity of the caisson obtained from the extraction test. Significant uplift of the caisson was observed when tensile loads up to 30 - 50% of the drained tensile capacity were applied in the previous research [24]. Thus, 30% of the drained tensile capacity was fixed as tensile amplitude in serviceability limit state. For storm loading, tensile loads of more than 50% of the drained tensile capacity were used. Details of each test and amplitudes in prototype scale is provided in Table 3.5.

Chapter 4

Finite Element Modelling

Soil profile in real scale problems varies widely in spatial manner and is rarely homogeneous throughout the problem depth. Therefore, extensive modelling (physical and numerical) is required to gain confidence in the design of the foundation. Research using physical models has the constraints of time and cost. Thus, Finite Element Modelling (FEM) is preferred to study the behaviour of soil for numerous scenarios by changing the model parameters. But, validation of models against experimental results is important to determine the usefulness of the software.

This chapter gives a brief insight into the FEM done in this thesis. Plaxis 2D was used to model the prototype behaviour of soil under cyclic loading as mentioned in the previous chapter. First, discretization of the problem is discussed followed by a section where the model parameters are discussed. It is followed by a discussion on the initial and boundary conditions and finally the loading scenarios in plaxis 2D are explained.

4.1 Model discretization

Using plaxis 2D, FEM was done for the problem discussed in the previous chapter. Since no horizontal loading components were applied and also due to the cylindrical geometry of the caisson, finite element analysis in this thesis was done in an axisymmetric way. Axisymmetric approach uses the rotational symmetry of the structure, where a two-dimensional input is analysed in a 3 dimensional manner. Using this approach, a cylindrical pie with an angle of 1 radian was analysed.

Parameter	Symbol	Value	Unit
Axial stiffness	EA_1	40E5	kN/m
Flexural rigidity	EI	40E3	kNm^2/m
Specific weight of material	w	8.560	$kN/m/m$

Table 4.1: Material parameters for suction caisson modelled in plaxis

Suction caisson was modelled as a stiff plate with material properties similar to that of the brass used in the centrifuge tests. Since the caisson lid was also considered as a stiff plate, point load applied through the guide rod in the centrifuge tests was modelled as a line load since the force was assumed to be distributed equally among the whole area of the caisson lid. Table 4.1 presents the material parameters of the suction caisson along with the specific weight of the material. Specific weight was calculated using density and volume of the material.

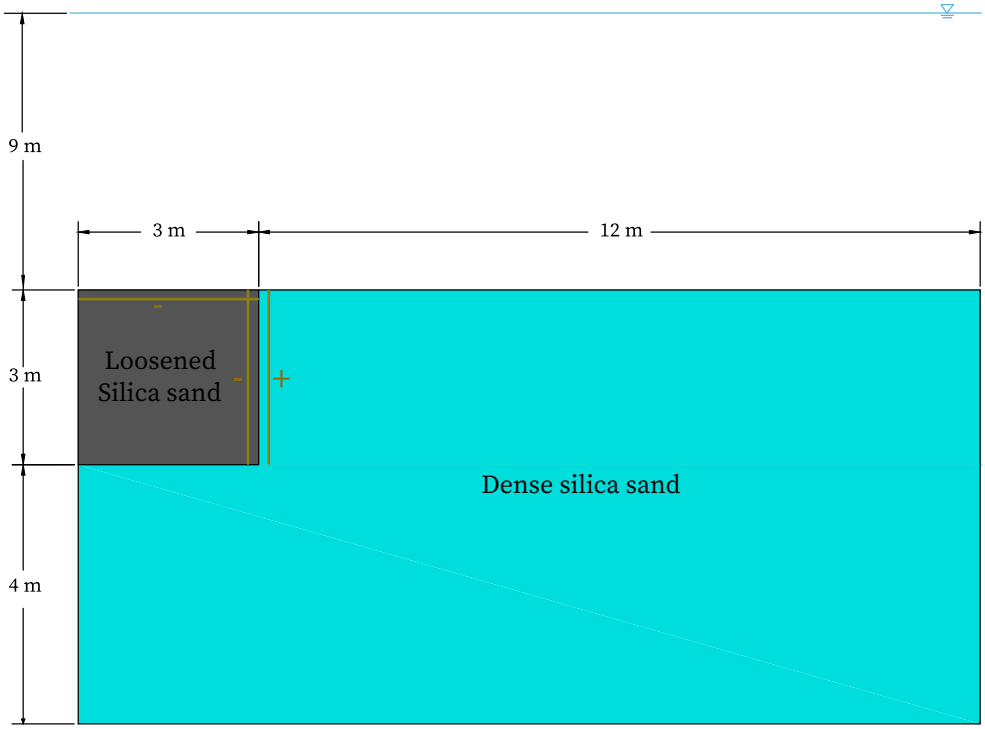

Figure 4.1: Geometry of the model defined in plaxis

Suction caisson was embedded in the homogeneous soil layer as denoted in Figure 4.1. Caisson was wished in place at the left corner of the soil volume. In all the suction caisson installation tests, it was noticed that, caisson penetration depth was never equal to the skirt length i.e. soil surface inside the caisson was above the surrounding soil surface due to heaving of soil. On visualising the installation process using Particle Image Velocimetry (PIV) analysis, it was understood that the sand inside the suction caisson had loosened and heaved due to the seepage flow that had occurred during suction installation phase. This phenomenon was witnessed by M.N. Tran (2005) [8]. This led to the reduction of density of sand inside the caisson. To model this behaviour in plaxis, a new sand was modelled with a reduced relative density of 35%. Numerous simulations were done using plaxis 2D to analyse the problem and to achieve convergence with the results obtained from the centrifuge modelling. All the simulations were done in four phases, namely,

- Phase 1: Initial phase was done using $K0$ procedure to generate the initial effective

stresses and state parameters.

- Phase 2 (Installation phase): In this phase, caisson elements were activated along with the positive and negative interface. Interfaces were added to model the soil-structure interaction properly. Hardening soil model was used in this phase as UBC sand model for installation phase provided unrealistic displacements during the cyclic loading phase. Since no waiting period was provided after each phase, calculation was done using plastic method.
- Phase 3: In this phase, soil was modelled using UBC sand model to provide continuity for cyclic loading phase. Also, loose sand inside the caisson was activated to model the real behaviour of suction installation.
- Phase 4: In this phase, vertical cyclic loads were applied in a pseudo static way at the center of caisson lid using UBC sand model. Calculations were done using plastic method.

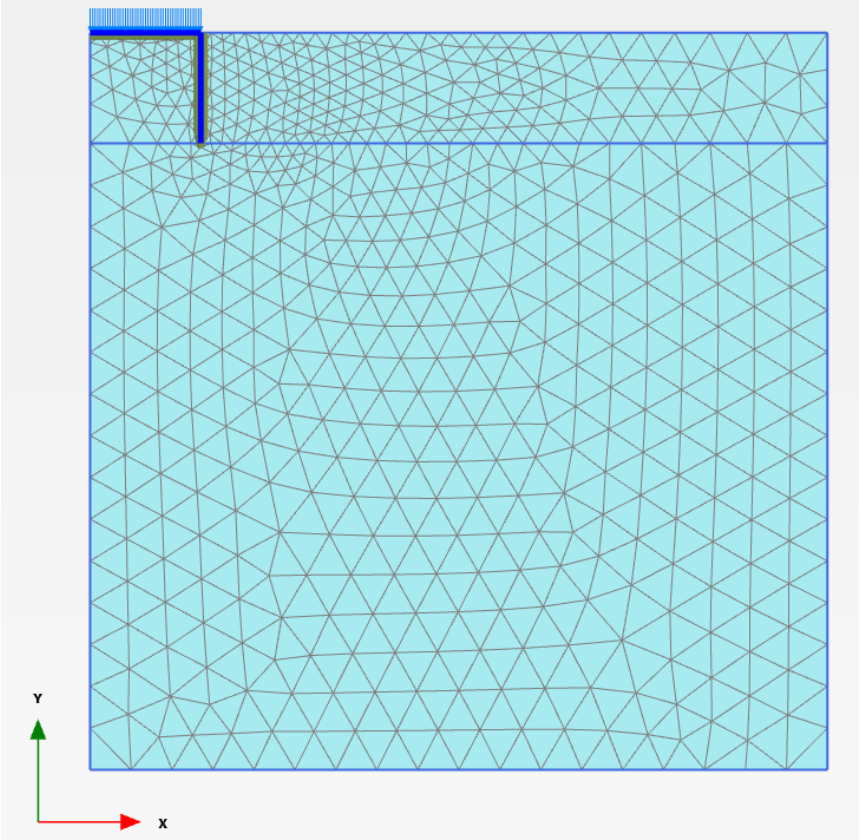

Figure 4.2: Generated fine mesh for the FEM simulation

A fine mesh was generated for this analysis using the built-in function in plaxis. Fineness of the mesh was 0.04 and it had 1226 elements with 10158 nodes. The mesh was finer around

the caisson causing the elements to be packed densely around the caisson and became coarser as the distance from the caisson increased. This gave better accuracy of results and also reduced the time required for analysis by reducing the number of nodes away from the point of interest. The generated mesh is given in Figure 4.2. These characteristics of mesh provided a better convergence of results when compared to coarser meshes.

4.2 Model parameters

Constituve soil models that can be used to analyse the application of cyclic loading in sand were discussed in Chapter 2. After detailed analysis of the available literature, UBC sand model was used to model the problem. As mentioned in the previous section, hardening soil model was used for the initial and installation phases. Literature on how to obtain the parameters for both the models is given in section 2.6. Strength parameters for silica sand were obtained from the direct shear test done in the laboratory. Calibration was done using this test data and Figure 4.3 shows the calibration graph for shear stress against normal stress. Calibration against shear strain was not possible as shear strain cannot be measured from a direct shear test as opposed to in a simple shear test available in Plaxis. Critical state friction angle obtained from direct shear test and plaxis soil tests matched really well and thus gave confidence in the soil parameters used in this analysis.

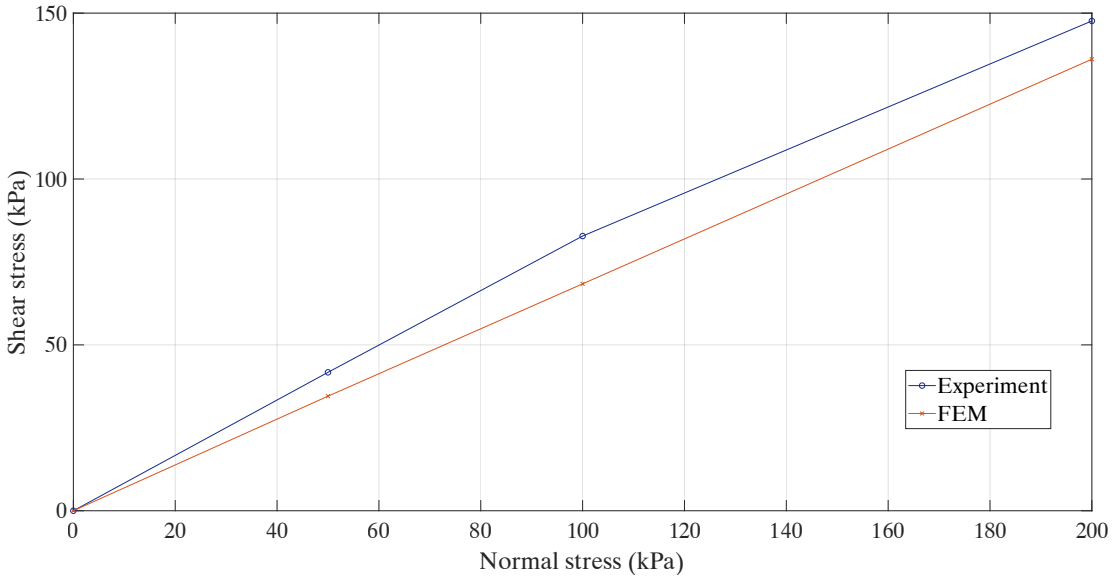

Figure 4.3: Parameter calibration for direct shear test

Stiffness parameters and other advanced parameters of the silica sand were obtained based on the correlations with relative density of the model prepared for the centrifuge tests.

Parameter	Symbol	Value	Unit
Angle of internal friction	ϕ_p	39.4	(°)
Secant stiffness	E_{50}^{ref}	45000	kN/m^2
Oedometer reference stiffness	E_{oed}^{ref}	45000	kN/m^2
Unloading/reloading stiffness	E_{ur}^{ref}	135000	kN/m^2
Power of stress-level dependency of stiffness	m	0.5	-

Table 4.2: Parameters for Hardening soil model

Relative density of the centrifuge samples was around 75%. In this thesis, all the plaxis simulations were run using the parameters obtained from a relative density of 75%. Input parameters for the hardening soil model and the UBC sand model are given in Table 4.2 and 4.3 respectively.

Parameter	Symbol	Value	Unit
Constant volume friction angle	ϕ_{cv}	34.1	(°)
Peak friction angle	ϕ_p	39.4	(°)
Elastic shear modulus	K_G^e	1269	-
Elastic plastic modulus	K_G^p	2479	-
Elastic bulk modulus	K_B^e	888	-
Elastic shear modulus index	ne	0.5	-
Elastic bulk modulus index	me	0.5	-
Plastic shear modulus index	np	0.4	-
Failure ratio	R_f	0.9	-
Reference pressure	P_{ref}	100	kN/m^2
Densification factor	fac_{hard}	0.3	-
SPT value	$(N1)_{60}$	25	-

Table 4.3: Parameters for UBC sand model

Stiffness parameters for the sand modelled to depict the loose sand inside the caisson is given in Table 4.4. Relative density of 35% was calculated for this sand by knowing the depth of heave of sand. Soil parameters were obtained using the same relative density correlation as above.

Parameter	Symbol	Value	Unit
Elastic shear modulus	K_G^e	763	-
Elastic plastic modulus	K_G^p	168	-
Elastic bulk modulus	K_B^e	534	-
SPT value	$(N1)_{60}$	5.44	-

Table 4.4: Stiffness parameters of loosened sand (UBC sand model)

4.3 Initial and boundary conditions

The soil volume was modelled as homogeneous in nature. This contradicts the real scale scenario, wherein homogeneity of the soil is quite rare. But due to complexity in modelling the heterogeneous soil, homogeneous soil was modelled in this thesis. Water level was kept 9 metres above the soil surface to simulate laboratory water pressures. Pore fluid used in the centrifuge tests was de-aired water and so very minute pore pressure was recorded in the sensor beneath the caisson lid in the centrifuge tests. This pore pressure value was negligible and thus, in plaxis, calculations for the problem were done in a drained manner. Also, as mentioned in the Section 4.1, initial phase was calculated using $K0$ procedure, which uses the friction angle and vertical stresses to calculate the horizontal stresses.

Boundary conditions
Boundaries of the model were assigned in a way to replicate the boundaries of strong box. The bottom boundary in Y axis was modelled as fixed to represent the bed rock or base of strong box. The top boundary in Y axis was set as free. Minimum boundary in X axis was modelled as normally fixed to represent a roller support. Maximum boundary in X axis was modelled as fixed to represent the lateral wall of strong box.

4.4 Loading conditions and scenarios

In summary for the centrifuge tests, suction caisson was installed in a strong box at laboratory conditions and behaviour of the caisson under cyclic loading was tested in the geo-centrifuge at an acceleration level of 100g. The compressive loading amplitude was chosen based on the buckling capacity of the guide rod and the tensile amplitude was chosen based on the drained tensile capacity. The frequency of loading was determined based on the loading actuator capacity. Various loading scenarios applied in the centrifuge are mentioned in Section 3.6.2.

In plaxis, one-way compressive loading with an average load of 250 kN and two-way symmetric loading with an average load of 0 kN were simulated. Even though few cyclic loading tests were done in layered sand in the centrifuge, all the centrifuge tests were not simulated in plaxis due to time constraint. Thus, both loading scenarios were tested only for the homogeneous soil profile. Loads discussed in Chapter 3 (prototype scale) were used as input for Plaxis.

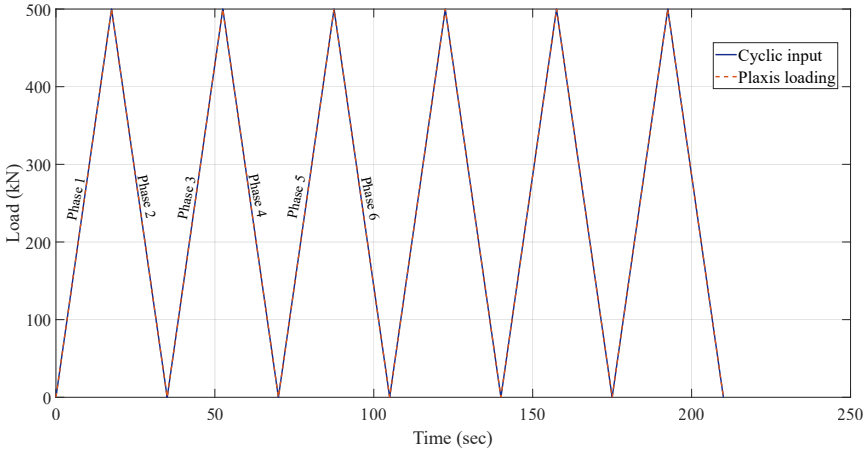

Figure 4.4: Static load discretized into two phases for each cycle of loading

Loads on a soil profile or a structure in plaxis can be applied in two ways; dynamic or pseudo static. Since frequency of the cyclic loads applied in this thesis was very low, dynamic behaviour was not witnessed in the centrifuge tests and thus, static loading was used. The static loads were applied as shown in Figure 4.4. Each cycle of the applied load had 2 phases in it. One phase consisted of the minimum amplitude and the other phase constituted the maximum amplitude. 1000 phases were created using staged construction to simulate 500 cycles of cyclic load. Both the loads were applied as a vertical component in F_y direction. Compressive loads were applied using negative sign and tensile loads were applied using positive sign. In the centrifuge, displacement of the caisson was measured at the center of the caisson. Since displacement behaviour of the caisson is compared with the FEM results, soil behaviour at the center of the caisson had to be studied in plaxis. Thus, a node was selected on the soil at co-ordinates (0.00, 0.00) and displacement graphs were plotted for the behaviour of soil at this node.

Chapter 5

Results and Discussions

In this section, results obtained from the installation tests done at 1g will be discussed first followed by the extraction test result and the cyclic loading test results, which were done in the centrifuge at 100g. Finally, validation results of FEM are discussed.

5.1 Installation

Installation tests in this thesis were done under laboratory conditions. Initially, installation was planned to be done at 100g. But could not be done as planned due to two reasons,

- Electric gear wheel pump used for installation did not operate in the centrifuge at higher acceleration levels. Due to the increase in the weight of all the components of pump inside the centrifuge, 12 V power supply was not enough to provide the necessary force to make the coil come in contact with the electrical circuit.
- In gravity flow, the pipe connecting the caisson and the reservoir passes over the wall of strong box in the shape of siphon, where water had to flow upwards first and then downwards. At higher gravity, since the weight of water had increased, more force was required for the upward flow of water. Since this force was not attained by the head difference, cavitation occurred inside the pipe at the siphon. This did not happen at laboratory conditions because the weight of water was less at normal conditions and head difference was sufficient to create the pressure required for flow of water. To overcome this problem, pipe should go through the wall of the strong box, rather than above the strong box wall. This would avoid the upward flow of water and thus cavitation can be avoided. Also, in order to attain a higher flow rate, water level in the reservoir should be kept constant.

In this section, installation results will be discussed for various scenarios. In all of the tests, initial caisson penetration of 10 mm was done using the load actuator to denote the self-weight penetration phase. Self-weight penetration was done at a very low rate of 0.05 mm/sec, to leave the soil sample undisturbed. It was noted that, if sufficient seal was not

provided during self-weight penetration phase, piping of soil occurred, causing a failure in installation. Contact between soil surface and caisson lid was realised when there was a sudden spike in the pressure sensor beneath the caisson lid and no displacement was recorded from LVDT. This denoted the completion of caisson installation. In this thesis, all installations were successful with no piping. Results discussed here represent only the suction assisted penetration phase. Suction data (s) is normalized against the effective unit weight of sand (γ') and diameter of the caisson (D), whereas penetration depth (z) is normalized against the skirt length (L) of caisson to provide a dimensionless comparison.

5.1.1 Effect of change in the flow rate using pump

In this section, the effect of flow rate on installation done using pump is explained. Flow rate of each test is mentioned in Table 3.4. Figure 5.1 shows the measured normalized suction against the normalized penetration depth of caisson during suction assisted installation. It also shows the predicted suction calculated using Houlsby & Byrne approach. On comparison with Houlsby & Byrne prediction model, it can be seen that suction pressure development trend is very similar to the one observed in the installation tests. As mentioned in Chapter 4, in all of the tests, caisson penetration depth was never equal to the skirt length of 30 mm (z/L = 1). This was due to loosening of the sand inside the caisson caused by seepage flow during suction assisted penetration. This in turn caused the sand to heave and thus pushed the soil surface inside the caisson slightly higher than the outer soil surface.

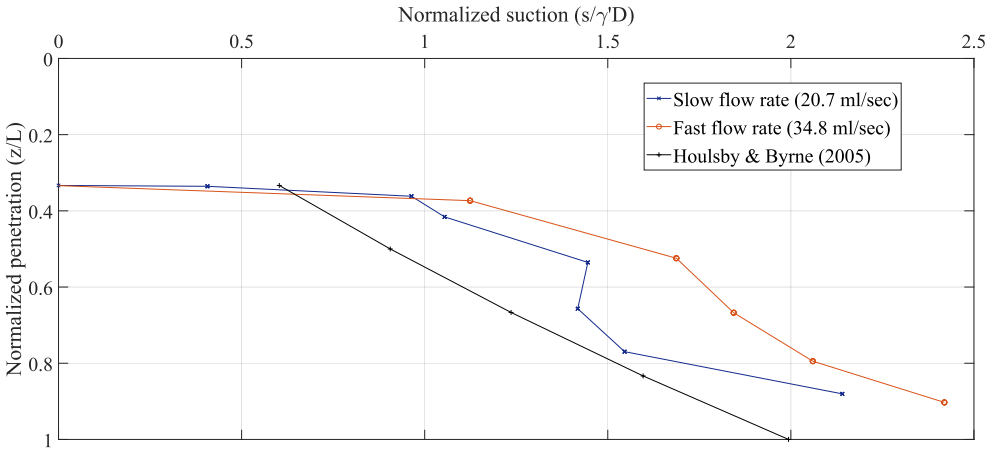

Figure 5.1: Normalized suction pressure acquired against the normalized penetration depth for varying flow rate using pump

It can be seen from Figure 5.1 that both the flow rates resulted in successful penetration of the caisson. Since the time taken for installation is around 2 seconds, more data points could not be recorded to obtain a smoother curve. For both the flow rates, there is a sharp increase in the suction initially without much penetration. This can be attributed to the

onset of seepage flow, which reduces the effective stress of soil at the tip and inside walls of the caisson and facilitates penetration of caisson. It is followed by a linear increase in the suction acquired with the penetration depth. As anticipated, there is a clear difference in the suction obtained for both the flow rates. This shows the dependence between the flow rate and the suction obtained as reported by M. N. Tran (2005) [8]. Despite the difference in flow rate, suction response is found to be similar for both rates with the faster flow rate having a slightly higher gradient.

5.1.2 Effect of change in the installation method

In this section, the results obtained from installation done using pump and gravity flow are discussed. Gravity flow had the lowest flow rate when compared to the flow rates obtained from the installation done using pump. Figure 5.2 provides a comparison of the suction acquired against the penetration depth for various scenarios tested in this section. It is important to remember that the flow rate acquired using gravity flow was not constant, but decreased with decreasing head difference between containers. Initial flow rate in the gravity flow was 25.17 ml/sec, which was higher than the flow rate obtained by slow installation done using pump (20.7 ml/sec). This caused an increase in the suction required for the onset of seepage flow. Since, fast installation using pump had a flow rate of 34.8 ml/sec, the suction acquired for the onset of seepage flow is more than that acquired in the other two tests. This explains that the flow rate has a direct effect on the suction required for the onset of seepage flow. All of the tests resulted in successful installation and the suction required for penetration increased linearly with respect to the penetration depth. This shows that, installation method does not have a significant effect on the installation process.

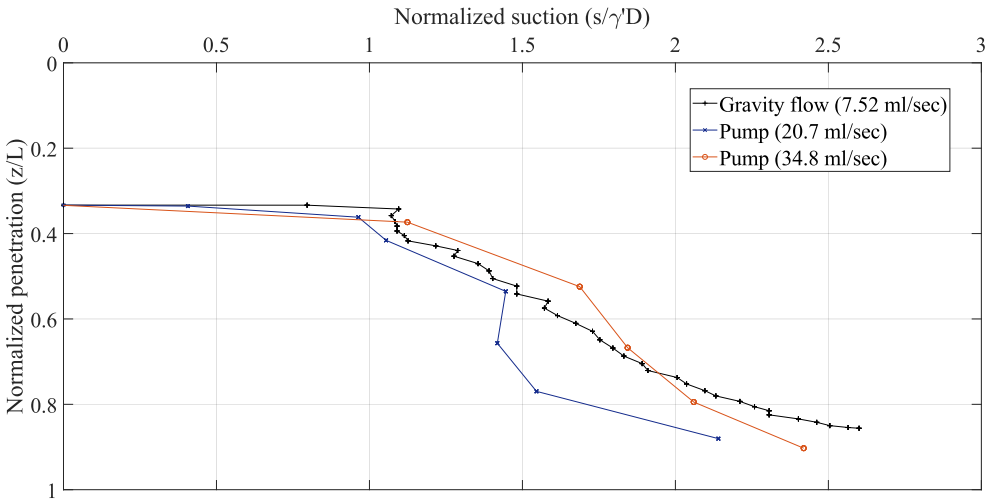

Figure 5.2: Normalized suction pressure acquired against the normalized depth of penetration for different installation methods

5.1.3 Effect of varying soil profile

This section investigates the effect of soil profile on suction installation. Geba sand with a permeability of 4.2E-5 m/sec was present on top of the silica sand with a permeability of 8.41E-4 m/sec as explained in Section 3.4. From literature, it was found that, installation in layered sand cannot be achieved when the flow rate is low. Thus, gravity flow was not used to install the caisson in layered sand. Installation was possible only using faster flow rate obtained using the pump. Figure 5.3 compares the installation data of homogeneous sand against layered sand. Permeability of geba sand is less than silica sand by a factor of 10. It can be seen from Figure 5.3 that the presence of a layer of less permeable sand clearly has an effect on the installation.

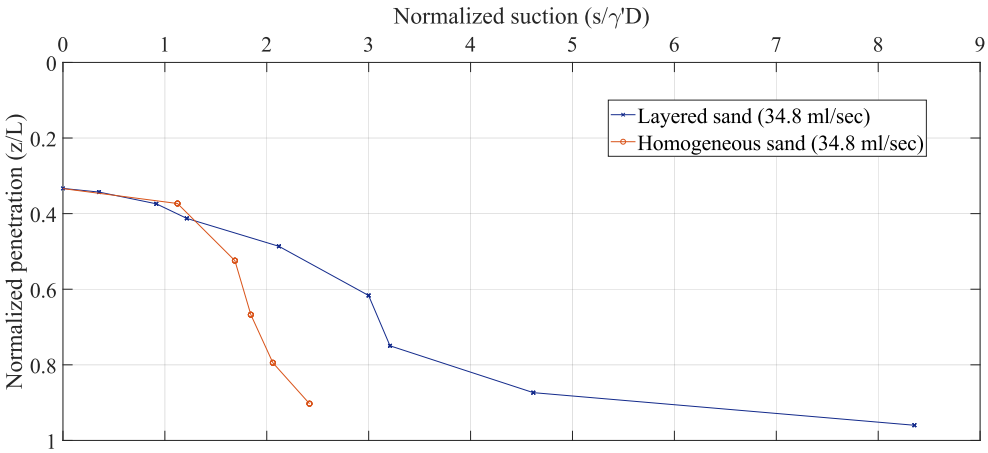

Figure 5.3: Normalized suction pressure acquired against the normalized depth of penetration for varying soil profile

Suction pressure required was higher than that required for installation in homogeneous sand. This was due to a hydraulic blockage created by the less permeable sand on the top which caused the need for more suction for installation to happen. It can be concluded that in the presence of a less permeable soil layer, the suction pressure required for installation is more than that required in the case of homogeneous sand by a factor of at least 3. This increase in suction caused more loosening of the silica sand and uplift of the geba sand layer.

Figure 5.4 shows the PIV analysis done during installation of a half caisson model by M.N. Tran [8] (Note: penetration is not complete). Similar difference in behaviour between the layered sand profile and homogeneous sand profile as observed in this thesis was observed by him. The three key observations in his research were:

- He observed that in homogeneous sand profile, a heave of approximately 2 mm was witnessed, whereas in layered sand profile, an uniform heave of around 4 mm was witnessed. Excess heave was formed in the homogeneous sand layer in layered profile.

- An uniform uplift of the less permeable sand layer inside the caisson due to the differential pressure was observed as is visible in Figure 5.4.
- He also witnessed scouring of the less permeable sand layer caused by the hydraulic flow path.

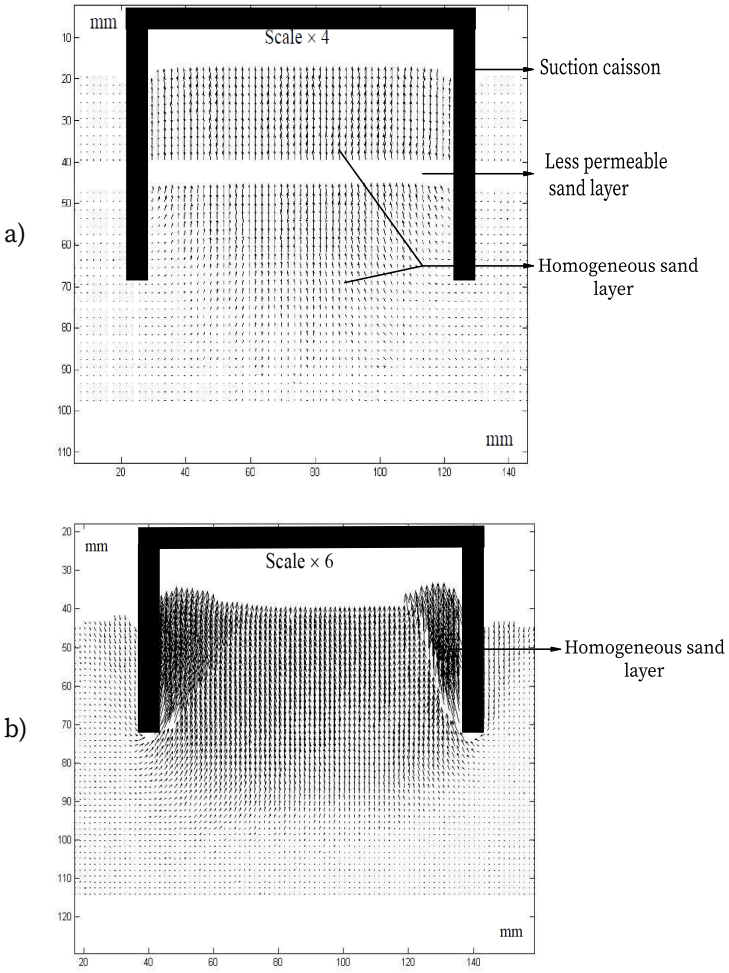

Figure 5.4: PIV output of soil deformation occurred during the suction caisson installation in a) layered sand profile b) homogeneous sand profile (from [8])

5.2 Extraction

To determine the drained tensile capacity of the caisson, slow extraction tests were done in the centrifuge at 100g. Hence, all the values in Figure 5.5 are given in the prototype scale. Extraction of caisson was also done after every cyclic loading test. It was observed

that the drained tensile capacity of the caisson did not vary much with the cyclic loading history. Tests were stopped once the tensile capacity was mobilised to save time. This was realised when the load reached a plateau or when the load started to reduce with increasing displacement as shown in Figure 5.5. Also, in the figure, the tensile capacity predicted by Houlsby & Byrne is provided. It can be seen that the prediction matches well with the experimental value. It was also noticed that the drained frictional resistance was mobilised within 0.15 m of upward displacement in all of the tests.

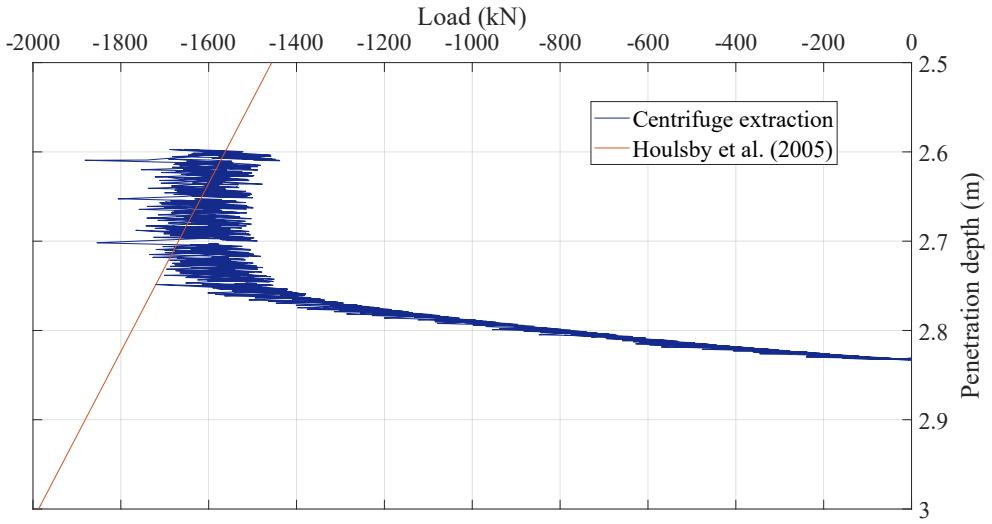

Figure 5.5: Drained extraction resistance plotted against the penetration depth

5.3 Cyclic loading

In offshore geotechnics, soil is always saturated with water level above the soil surface. In this thesis, due to the use of water as a pore fluid in the centrifuge at 100g, the behaviour of soil under cyclic loading is analysed as drained in the silica sand applications. Also, based on the recorded pore water pressure developed under the caisson lid, it was noted that little pore pressures of 0.01 kPa were developed for each cycle in the silica sand. This indicates that the behaviour is almost drained. But, when geba sand layer was present, a little higher excess pore pressure was recorded as will be discussed in Section 5.3.5. In all the tests, except in storm loading, one-way compressive loading represents the loading amplitudes from 0 kN to 500 kN and two-way symmetric loading represents the loading amplitudes from -500 kN to 500 kN. In this section, settlement or displacement response of caisson is discussed for various scenarios as it plays an important role in the overall serviceability of the structure. Displacement of 0 mm (y-axis) in the plots denote the initial position of the caisson before any cyclic loading was applied i.e. after the installation of the caisson. Also, stiffness response for varying scenarios is explained as it is critical for the calculation of natural frequency and fatigue design of foundations [24]. In every result discussed in

this section, settlement is represented by positive displacement and uplift of the caisson is represented by negative displacement.

5.3.1 Effect of average load on the cyclic behaviour of homogeneous sand

Settlement behaviour

Soil cannot sustain tension. Tensile capacity of a caisson is obtained by the frictional resistance offered by the walls and the negative pore pressure under the caisson lid in the case of undrained or partially drained behaviour whereas only by the skin friction in the case of drained behaviour as explained in Chapter 2. In two-way symmetric loading (average load = 0 kN), during tensile loading, upward movement of caisson was witnessed due to the reduction in frictional resistance offered by the caisson walls and this resulted in shearing of sand at the interface. This caused the sand to loosen which in turn caused increased settlement when compressive load was applied in the next cycle. Thus, settlement of the sand is higher in two-way symmetric loading when compared to one-way compressive loading (average load = 250 kN) as shown in Figure 5.6. In one-way compressive loading, the settlement of sand was caused only by the compressive forces and densification of sand due to the compressive loads. Since load applied was very low when compared to the bearing capacity of the foundation, settlement attained as a whole was less. Also, no accumulation of displacement was observed after about 200 cycles. This denotes that the skin frictional resistance was completely mobilised in 250 kN average load test after 200 cycles. In two-way symmetric load, resistance was not completely mobilised and hence, very slight increase in the settlement can be seen till the end.

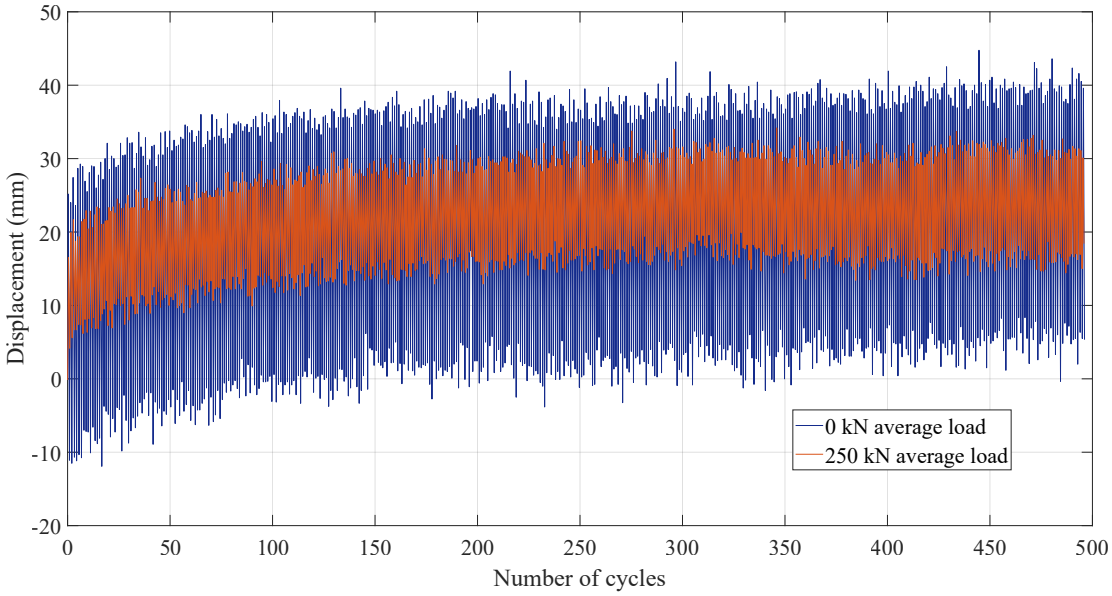

Figure 5.6: Displacement behaviour of the suction caisson under varying average load

Stiffness behaviour

Unloading stiffness is calculated by obtaining a slope between the maximum load point of the previous cycle and the minimum load point of the next cycle as shown in Figure 5.7.

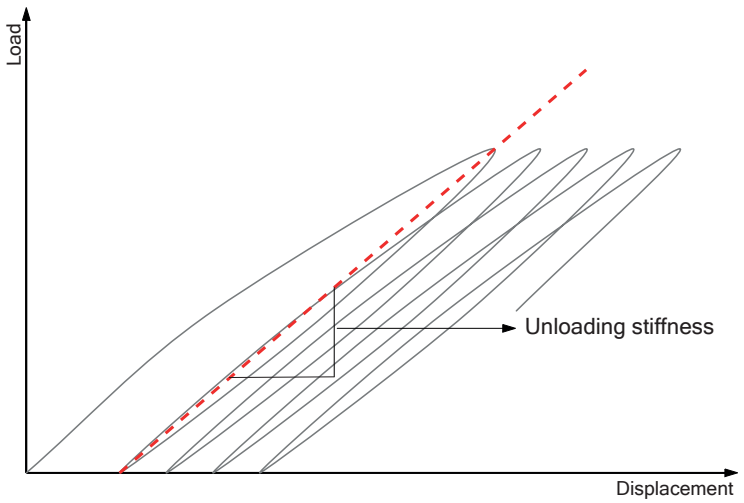

Figure 5.7: Illustration of the definition of unloading stiffness

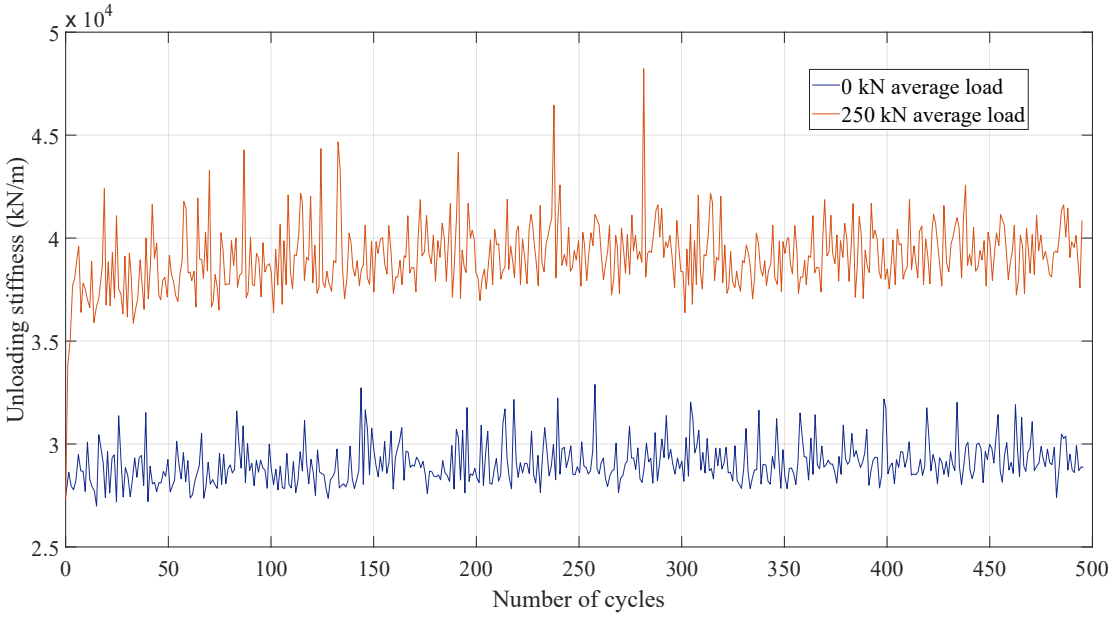

Figure 5.8: Unloading stiffness behaviour of the suction caisson under varying average load

Byrne and Houlsby (2004) mentioned that the stiffness of soil under cyclic loading increases with increase in the average load [17]. As illustrated in Figure 5.8, in one-way compressive loading, unloading stiffness of sand increases drastically in the initial few cycles before becoming constant or increasing at a very low rate. In two-way symmetric loading, there is

no drastic increase in the stiffness, but stiffness kept increasing very slowly with the increase in number of cycles. Since the stiffness of soil reduces with the introduction to tensile loading, displacement amplitude per cycle increased. Also, the average load decreases with the introduction of tensile component in loading. This shows that displacement amplitude per cycle increases with decrease in the average load. In both the cases, shake down behaviour was witnessed, which is explained briefly in the next section. This shows that the change in the average load affects only the overall settlement behaviour and not the behaviour of cyclic accumulation of displacement.

5.3.2 Effect of frequency on the cyclic behaviour of homogeneous sand

Settlement behaviour

Frequency at which cyclic loads are applied plays an important role in the soil behaviour. In this thesis, frequency used in all of the tests was 0.028 Hz (in model scale), which denotes the high frequency applied in this section. One test with a lower frequency of 0.014 Hz in model scale was done to study the effect of frequency variation on soil behaviour. Low frequency test was done only up to 300 cycles due to constraints in running the centrifuge after laboratory hours. Loads applied for these two tests were two-way symmetric loading with an average load of 0 kN. As explained in the previous section, when tensile loads were applied, resistance to the caisson uplift was offered by the frictional forces acting on the walls of caisson. When the caisson uplifted due to the tensile load, this frictional resistance tended to reduce at the interface which caused the sand to shear. Loosening or rearrangement of soil fabric occurred due to shearing. Thus, in the next compressive loading cycle, more settlement was witnessed. This will happen till the stiffness of soil is mobilised.

When the frequency of loading was lower, more time was taken to reach the tensile amplitude during loading. This in turn caused more shearing and thus the sand loosened even more. This resulted in an increased settlement when compared to higher frequency load. Thus, accumulation of displacement increases with decreasing frequency [25]. Since both the frequencies tested in this thesis were very low when compared to real conditions and were not dynamic frequencies, strain accumulation was plastic in nature [26]. In low frequency loading, it can be seen from Figure 5.9 that the accumulation of displacement with each cycle kept on increasing till the end of the test. This behaviour is known as ratcheting. Whereas, in the high frequency loading, the incremental cyclic displacement tends to reach a value of almost zero after about 150 cycles. This behaviour of soil is known as shake down behaviour, where, when a soil model is subjected to repetitive cyclic loading, accumulation of displacement with each cycle decreases, tending towards an asymptotic value [27]. Also, pore pressure behaviour was analysed for this scenario. It was observed that very minute pore pressures of 0.03 kPa developed for each cycle and thus would not have any significant effect on the foundation behaviour (refer Figure B.1).

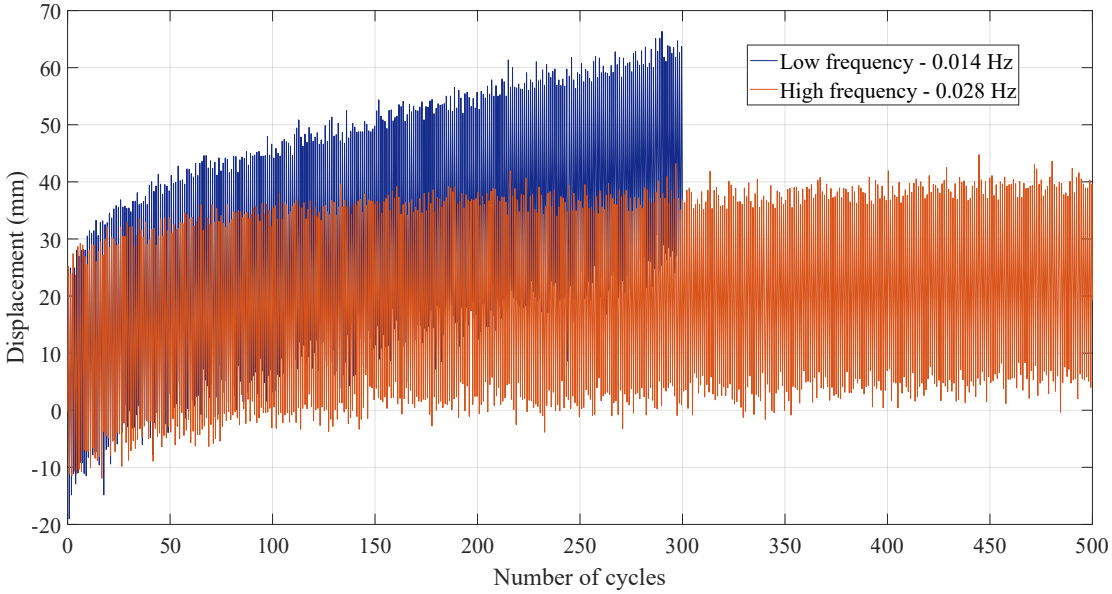

Figure 5.9: Displacement behaviour of the suction caisson under varying frequency

Stiffness behaviour

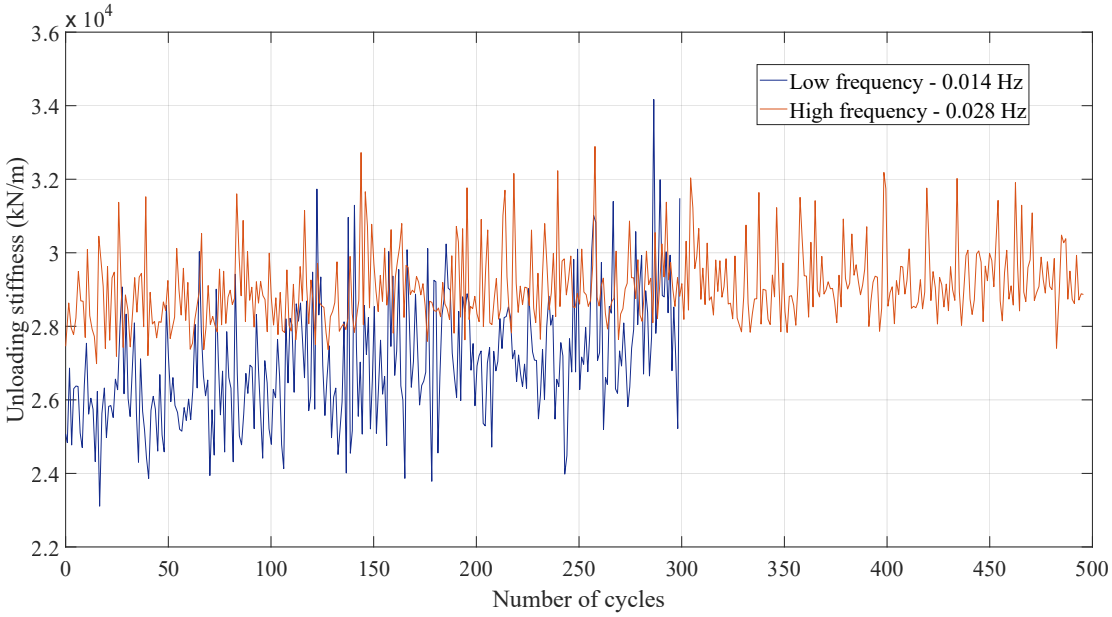

Figure 5.10: Unloading stiffness behaviour of the suction caisson under varying frequency

On studying the unloading stiffness characteristics in Figure 5.10, it can be said that the initial stiffness is lower in low frequency loading compared to high frequency loading. But, the rate of increase of stiffness per cycle in low frequency loading is much higher than that in the high frequency loading. This attributes to the increased rate of accumulation of plastic

strain in low frequency loading which was due to the excessive settlement that occurred in the model when compared to the high frequency loading. The excessive displacement was caused by the loosening and restructuring of soil particle due to the increase in time taken to reach tensile loading as explained in the previous section.

5.3.3 Effect of storm loads on the cyclic behaviour of homogeneous sand

Settlement behaviour

Under storm conditions, the amplitudes in tension and compression were varied with each packets of loading. Load amplitudes against the number of cycles in each packet are given in Figure 5.11.a) and Table 5.1. Figure 5.11.b) provides the displacement behaviour of the caisson for varying cyclic amplitudes. Average load for each cyclic amplitude packet is also mentioned. Till 300 cycles, compressive load amplitude was kept constant at 500 kN and the tensile load amplitude was increased. When the tensile amplitude was less than or equal to 50% of the drained tensile capacity (850 kN), caisson uplifted up to 1 cm. When the tensile load exceeded 50% of the drained tensile capacity (1100 kN), larger uplift of caisson was observed. Uplift increased by a factor of 2. When the average load was increased after 310 cycles by increasing the compressive load with a constant tensile load of 1100 kN, settlement of the caisson increased and decrease in the caisson uplift was observed. With increasing average load, an increased settlement was witnessed. It was concluded that, if the cyclic amplitude increases with a constant average load and drainage condition is predominantly drained, more settlement will be attained.

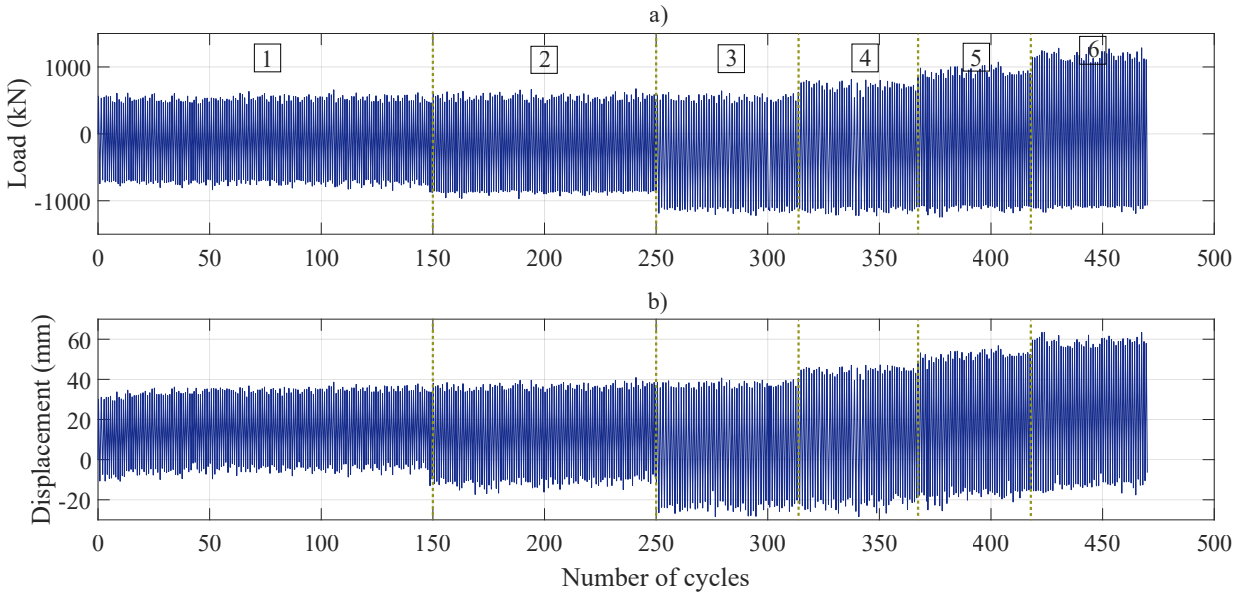

Figure 5.11: a) Load applied against number of cycles for each loading packet b) Displacement behaviour corresponding to each loading packet

Load packet	Max. amplitude (kN)	Min. amplitude (kN)	Initial cycle (-)	Final cycle (-)
1	500	-700	0	150
2	500	-850	151	250
3	500	-1100	251	310
4	750	-1100	311	365
5	900	-1100	366	410
6	1100	-1100	411	470

Table 5.1: Variation of loading amplitudes against the number of cycles for storm condition

Stiffness behaviour

Unloading stiffness, as seen in Figure 5.12, decreased with a decreasing average load. Within each cyclic amplitude packet, there was a slight increase in the unloading stiffness. When the average load decreased, the stiffness behaviour shifted to a lower magnitude instantly and remained constant or showed a slight increase in that packet. It can be noted that, at 250 cycles, there is a tremendous drop in the stiffness. This is attributed to the introduction of tensile load which was higher than 50% of the drained tensile capacity. Once the compressive load amplitude was increased after 310 cycles, the stiffness of the soil started to increase at a considerable rate which kept on increasing as a function of average load for the successive packets of cyclic amplitudes.

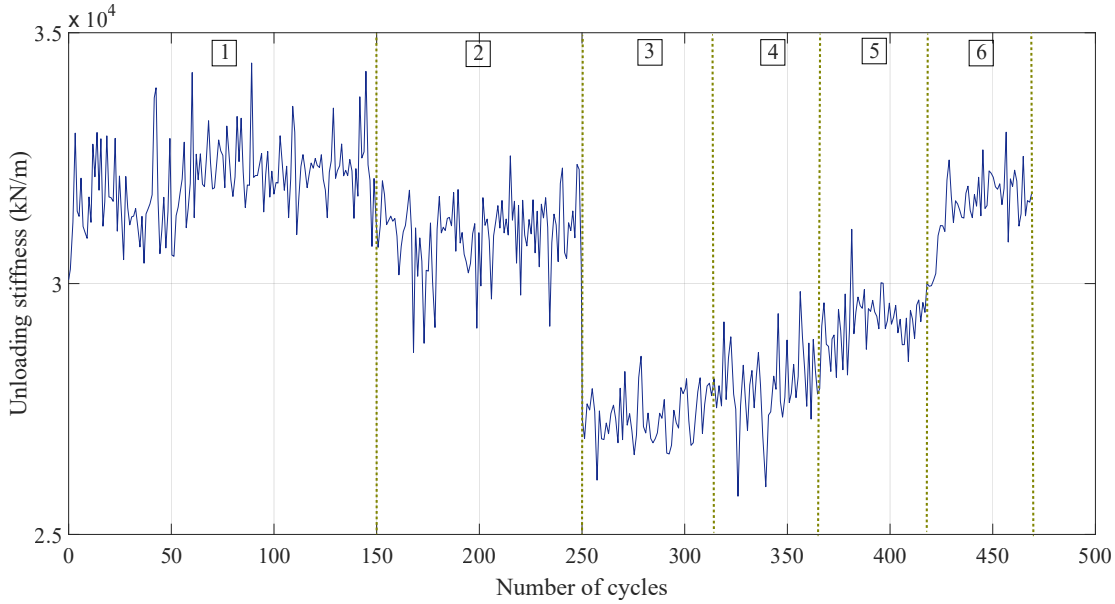

Figure 5.12: Unloading stiffness behaviour under storm loading

5.3.4 Behaviour of layered sand under one-way compressive cyclic loading

Settlement behaviour

In layered sand profile, the behaviour of the caisson was similar to that in the homogeneous sand profile with a slightly increased settlement until 210 cycles as can be seen in Figure 5.13. Silica sand in the layered sand profile gets compressed more compared to that in homogeneous sand profile. This can be attributed to the increased loosening of silica sand in the layered sand profile when compared to the homogeneous sand profile as the suction pressure required for installation in the layered sand increased due to the presence of hydraulic blockage caused by the less permeable geba sand layer. As explained in the homogeneous sand profile, cyclic loading caused the skin friction to degrade with each cycle. It was pretty evident during the initial few cycles, where settlement of the caisson can be witnessed. Thus, initial settlement was caused by the compression of silica sand beneath the less permeable geba sand layer.

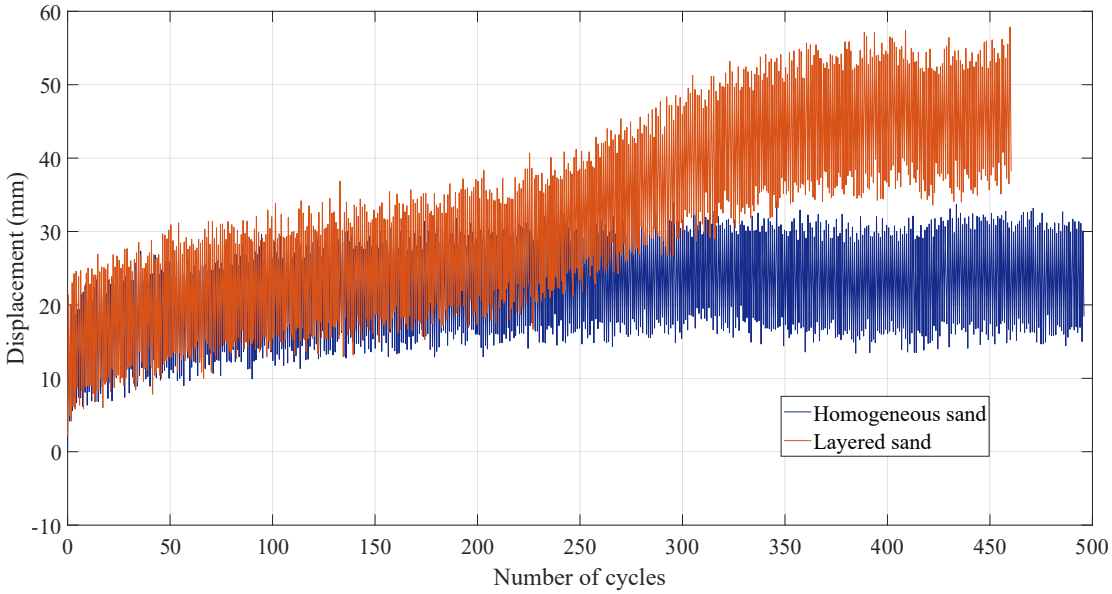

Figure 5.13: Displacement behaviour of the suction caisson under one-way compressive load for varying soil profile

Once the settlement of the soil profile became stable after 210 cycles, an excessive accumulation of displacement was observed for a period of 150 cycles as shown in Figure 5.13. This behaviour was not observed in the homogeneous sand profile and can be explained based on the observations made by M.N. Tran, presented in Section 5.1.3. Once the resistance offered by the silica sand was mobilised, the uplifted scoured plug started to compress due to compressive loading. This caused a tremendous increase in settlement. Once the frictional resistance offered by the geba sand layer was mobilised, no more accumulation of displacement was observed with the increase in the number of cycles. To gain confidence

in this result, the test was repeated, and a very similar behaviour was observed in the repeated test (See Appendix B.3.3).

Stiffness behaviour

Figure 5.14 shows the stiffness behaviour for homogeneous and layered sand profiles under one-way compressive loading. It can be seen that the stiffness of layered sand was lower than that of the homogeneous sand and this explains the slightly higher settlement in layered sand until 210 cycles. After 210 cycles, unloading stiffness of the soil system as a whole reduced at a faster rate. This was related to the increase in settlement due to settlement of the less permeable soil plug. Once the plug settled completely, stiffness behaviour became constant again.

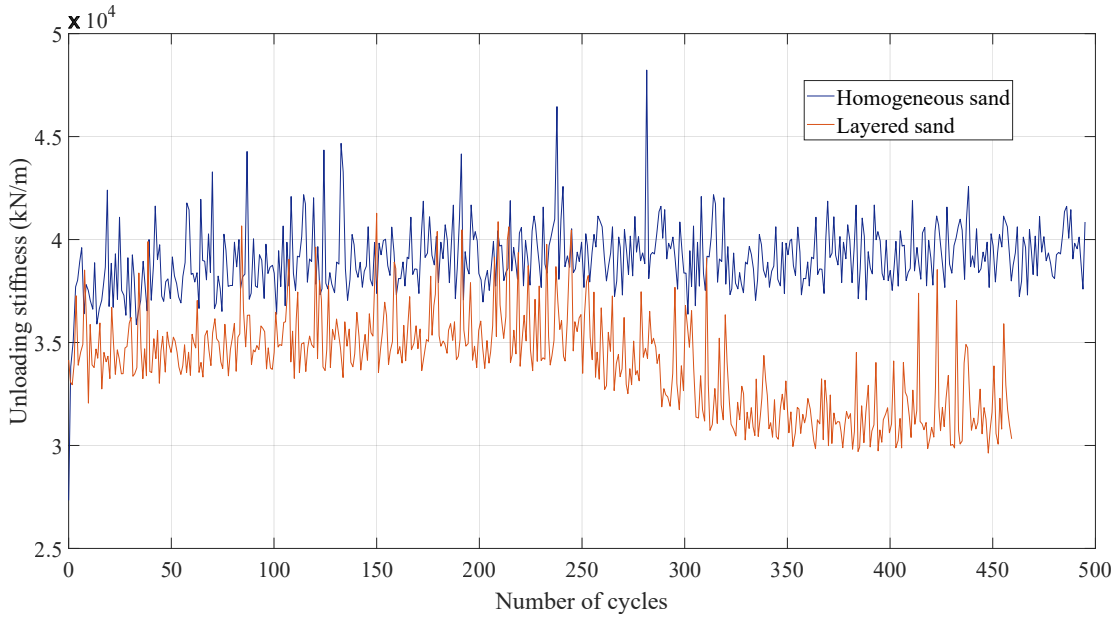

Figure 5.14: Unloading stiffness behaviour of the suction caisson under one-way compressive load for varying soil profile

5.3.5 Behaviour of layered sand under two-way symmetric cyclic loading

In two-way symmetric loading, the behaviour of caisson is similar in both homogeneous and layered sand as shown in Figure 5.15. As mentioned in Section 5.3.1, the settlement of soil increases due to the introduction of tensile loads and a similar settlement behaviour was observed in the layered sand. Also, uplift of the caisson was less in the layered sand profile when compared to the homogeneous sand profile during tensile loading. This can be explained with the help of excess pore pressure behaviour given in Figure 5.16. Even though very less excess pore pressures were developed in both the tests, on comparison, it can be

noted that the negative pore pressure obtained in the layered sand is higher than that obtained in the homogeneous sand. This might provide a little additional tensile capacity by the application of suction under the caisson lid. The increased negative excess pore pressure was due to the decreased permeability of the geba sand. In two-way compressive loading, as the stiffness of the silica sand layer was not completely mobilised, a drastic increase in settlement was not attained as witnessed in the previous section.

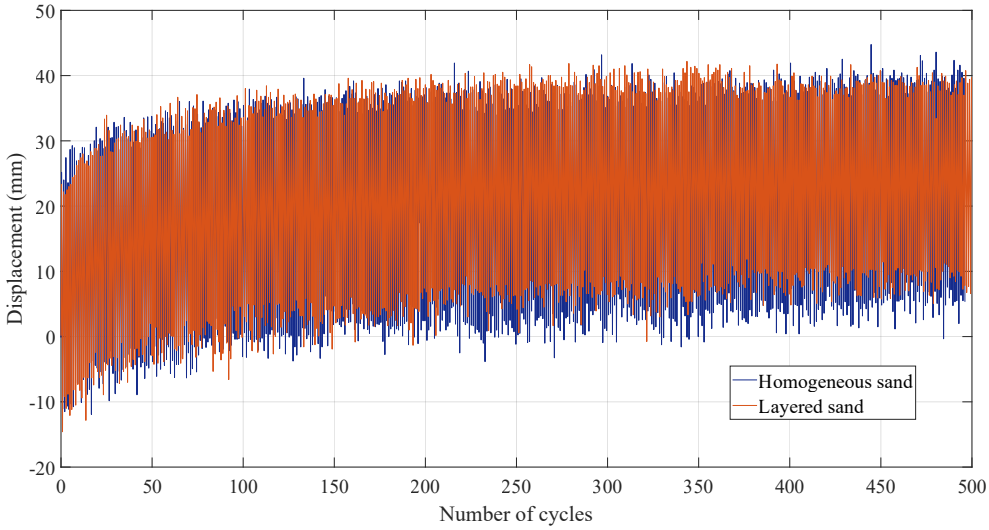

Figure 5.15: Displacement behaviour of the suction caisson under two-way symmetric load for varying soil profile

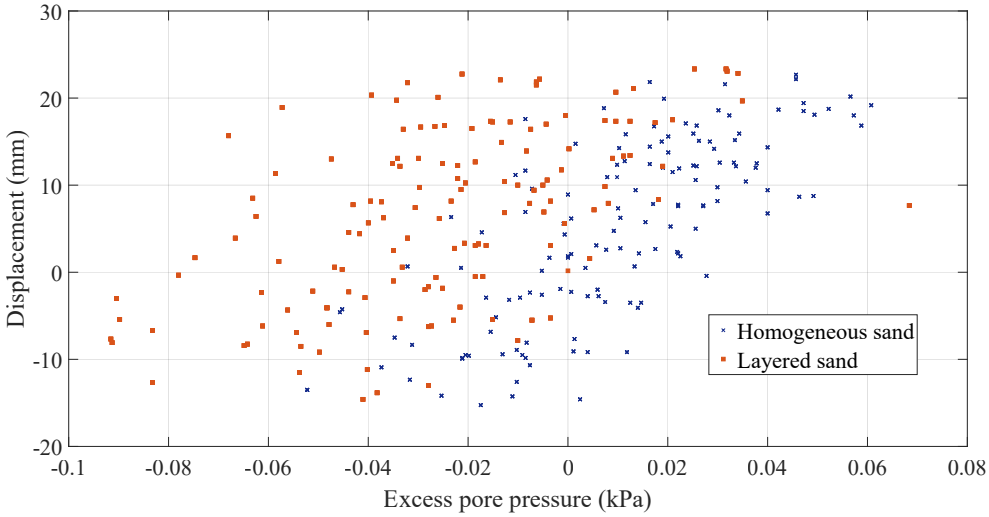

Figure 5.16: Pore pressure behaviour for initial few cycles under the caisson lid upon two-way symmetric loading in varying soil profile

5.4 Plaxis results

Problem geometry and silica sand used in the centrifuge tests were modelled in Plaxis to study the behaviour of caisson under cyclic loads using FEM. Details of the soil and model parameters used are given in Chapter 4. In this section, comparison of the displacement and secant stiffness behaviour in the centrifuge and the FEM is discussed. Comparison of unloading stiffness is not done due to the significant difference in displacement amplitudes. This causes very high stiffness in FEM when compared to the centrifuge. Only one-way compressive loading and two-way symmetric loading scenarios in the homogeneous sand was modelled due to time constraint.

5.4.1 One-way compressive loading

In this section, a comparison between the centrifuge and FEM simulation results for one-way compressive loading is provided. Cyclic displacement in the centrifuge along with the average displacement and the displacement obtained in FEM is given in Figure 5.17. It should be noted that, displacement obtained from FEM is not monotonic. But, the displacement amplitude in a cycle for FEM is less than that obtained in the centrifuge by a factor of 10. Reason for this behaviour is not known yet and needs further research. It can also be noted that, the displacement behaviour is similar in both physical modelling and FEM up to 150 cycles, after which, settlement in FEM keeps on increasing till the end of the simulation. On the other hand, the centrifuge displacement reaches a stable value and the rate of accumulation of displacement becomes zero. Plaxis model failed to capture this behaviour. Rather, ratcheting behaviour was witnessed, where upon repetitive loading, accumulation of displacement of the soil kept on increasing till the end of simulation.

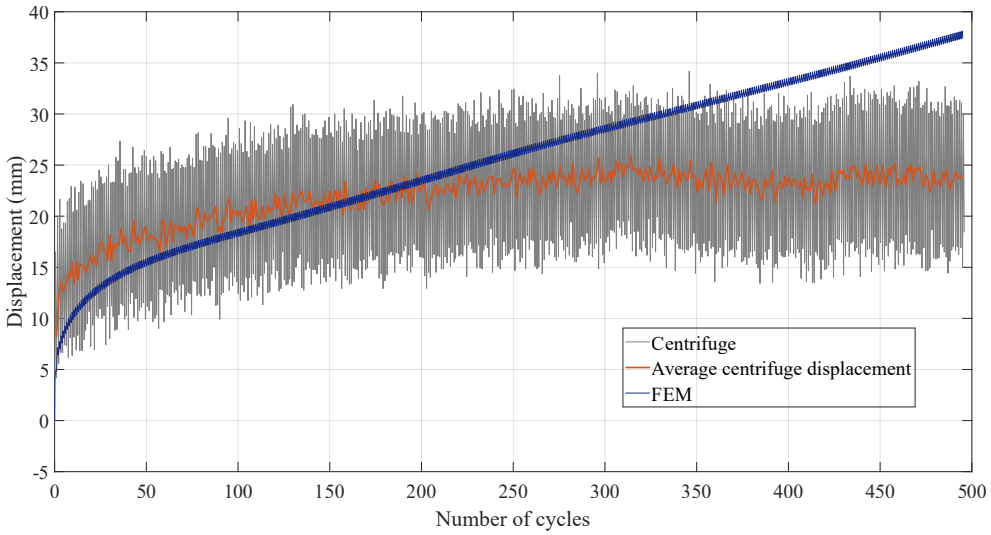

Figure 5.17: Displacement behaviour of caisson in the centrifuge and FEM under one-way compressive loading

Figure 5.18 shows the secant stiffness behaviour obtained from FEM and centrifuge tests. Initial stiffness observed in FEM was very high due to the large difference in the maximum displacement amplitude between the centrifuge result and FEM result in the initial few cycles. As settlement increases in FEM, the maximum displacement amplitude in FEM progressed towards the maximum displacement amplitude per cycle in centrifuge test, causing secant stiffness in FEM to become almost the same as in the centrifuge at the 340^{th} cycle. After 340 cycles, the settlement in FEM is higher than that obtained from the centrifuge. Thus, secant stiffness in FEM decreases below the centrifuge secant stiffness and follows a continuous decreasing trend.

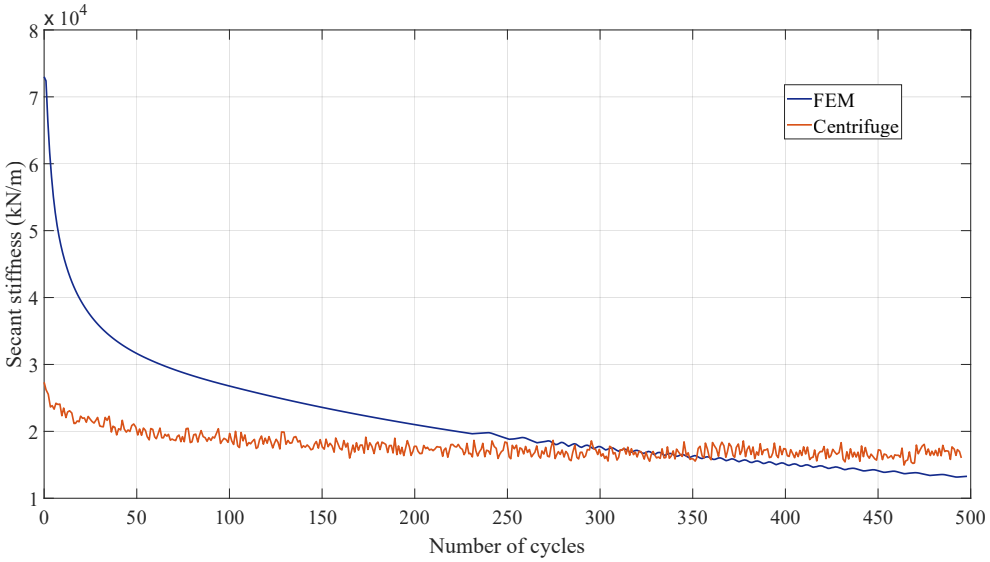

Figure 5.18: Secant stiffness behaviour of soil in the centrifuge and FEM under one-way compressive loading

5.4.2 Two-way symmetric loading

In this section, two-way symmetric loading result obtained from the FEM simulation is discussed. As can be seen from Figure 5.19, the settlement obtained is more than that obtained in the centrifuge modelling. Even in the initial 100 cycles, the settlement obtained in FEM is higher compared to the centrifuge. This difference may be due to the completely drained analysis done in plaxis whereas minute pore pressures were obtained in centrifuge. Following 100 cycles, minute accumulation of displacement was observed in the centrifuge tests as the cycles progressed. Whereas, in FEM simulation, after 100 cycles, a drastic accumulation of displacement was witnessed as the number of cycles progressed which led to very high settlement at the end of the test. Figure 5.20 gives the secant stiffness behaviour for both FEM and centrifuge tests. As illustrated in the previous section, the initial secant stiffness is very high in FEM due to very low maximum displacement amplitude when

compared to the centrifuge. Similar stiffness behaviour was observed in both one-way compressive loading and two-way symmetric loading scenarios.

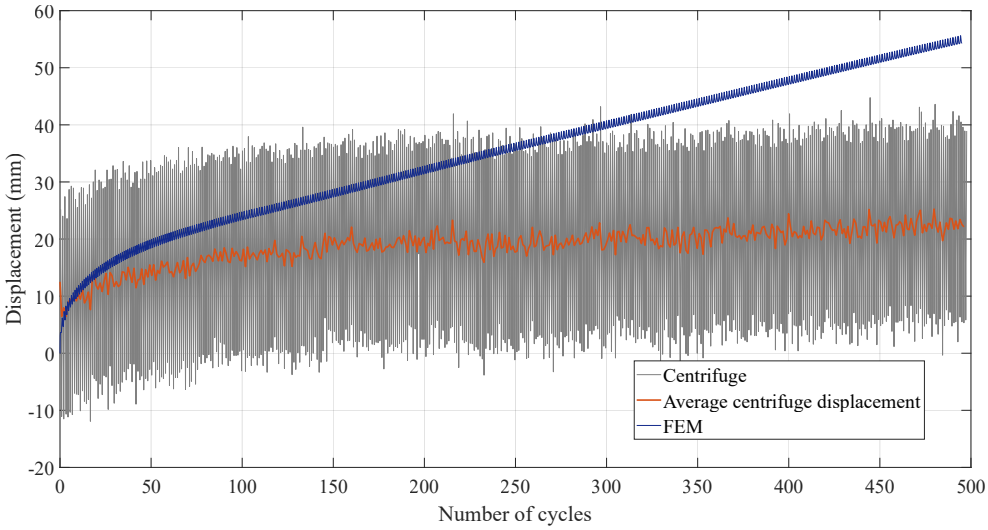

Figure 5.19: Displacement behaviour of caisson in the centrifuge and FEM under two-way symmetric loading

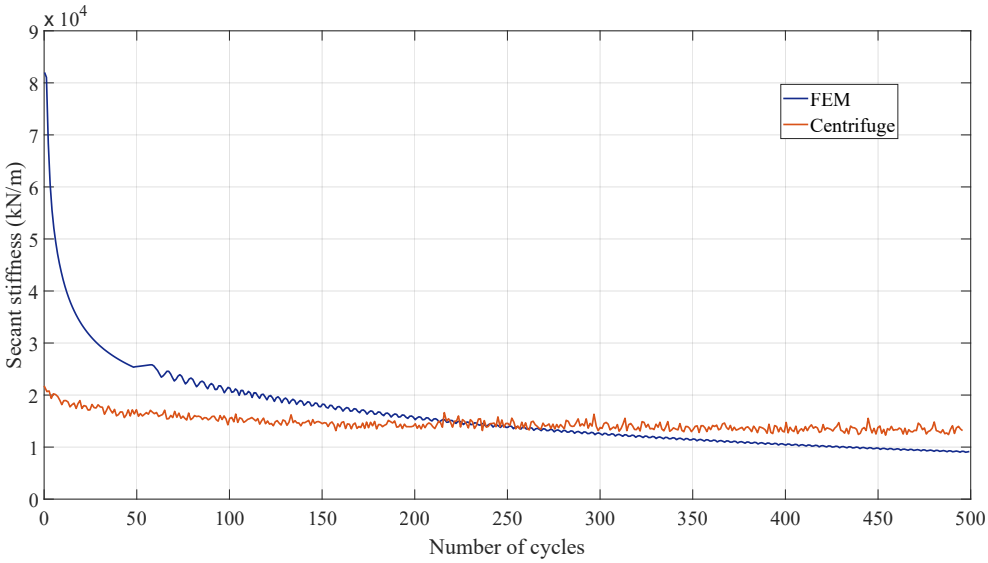

Figure 5.20: Secant stiffness behaviour of soil in the centrifuge and FEM under two-way symmetric loading

Chapter 6

Conclusions and Recommendations

6.1 Conclusions

In this research, various aspects of the suction caisson behaviour were analysed. First, installation behaviour was studied using a suction installation apparatus. Suction required for installation was applied using a discharge pump or with the aid of gravity flow to study the effect of installation method. Different flow rates and soil profiles were tested. Main conclusions obtained from this part of the study are summarized below.

- Flow rate had a clear effect on the suction acquired during installation. Higher the flow rate, higher the suction acquired. Also, an increase in flow rate resulted in an increased in suction required for onset of seepage flow.
- Although suction installation in a real scenario is done only using a pump, various methods are available for the application of suction at laboratory scale. It was noted that change in the installation method had no significant effect on the installation process, as long as sufficient flow rate was obtained.
- In the presence of a 10 times less permeable sand layer on top of a coarser sand, suction required for the installation increased by a factor of 3 when compared to installation in a homogeneous coarser sand profile.

Cyclic loading tests were done for varying load amplitudes to study the effect of average load on foundation behaviour. It was followed by a study on the effect of frequency on two-way symmetric loading. Also, the effect of storm loading conditions was analysed by using high tensile loads. Finally, the behaviour of layered sand under one way compressive and two-way symmetric loading was studied. Upon studying the stiffness response of foundation for various characteristics of cyclic loading, it can be concluded that selecting a representative stiffness for design purpose is very complex. Findings from all these tests are presented here:

- Introduction of tensile loads leads to an increase in the settlement of caisson. Also, initial unloading stiffness decreased with the introduction of tensile loads and further remained either constant or increased slightly throughout the cyclic load packet.

- When the frequency was changed, a clear difference was observed in the soil behaviour. Settlement increased drastically with the decrease in frequency. Initial unloading stiffness was less in the low frequency loading when compared to the high frequency loading and further increased with increasing number of cycles in low frequency loading.

- Significant uplift of caisson was witnessed when the tensile load amplitude was equal to 50% of the drained tensile capacity after which, double the amount of uplift was observed when tensile load was more than 50% of the tensile capacity. Stiffness of the caisson decreased with increasing tensile load.

- When the cyclic amplitude was increased at a constant average load, an increased settlement response was observed if the drainage condition was predominantly drained.

- Application of one-way compressive load on layered sand revealed that the initial settlement behaviour was similar to the homogeneous soil layer. But a drastic increase in the settlement was witnessed once the stiffness of the more permeable soil layer was mobilised. This was due to the compression of the less permeable sand layer on top of the more permeable sand layer.

- On application of two-way symmetric load on the layered sand, a slight increase in the tensile capacity was observed due to the development of minute negative excess pore pressures or suction beneath caisson lid. In case of an undrained scenario, the tensile capacity of the caisson will be significantly higher.

Finally, the results obtained from the centrifuge were compared with the results obtained by modelling a similar problem in geotechnical finite element software, plaxis 2D. It was noticed that the initial behaviour of sand was similar for both one-way compressive and two-way symmetric loading scenarios. But after that, it was noticed that the shake down behaviour of soil was not captured in finite element modelling. This may pose some serious problems in the design of caisson as the long-term settlement behaviour is very important for serviceability conditions of the foundation.

6.2 Recommendations

- Installation behaviour at higher acceleration levels should be studied by making the modifications suggested in this thesis. This helps in better realisation of installation process at prototype level.

- Centrifuge tests should be done with samples prepared using viscous fluid to study the undrained or partially drained behaviour of sand. This helps in understanding the role of pore pressure in the response of the foundation.
- More tests can be done in layered sand by varying the less permeable sand layer depth or position. Also, layered soil profile with clay and sand can be studied to further model and understand the behaviour of caissons in real conditions in North Sea.
- Incorporation of shake down behaviour of soils in the constitutive models on cyclic loading applications is very important to obtain a real soil behaviour and further gain confidence in the FEM results.

Appendix A

Data regarding the laboratory tests done on soils to obtain the properties is given in this section.

A.1 Direct shear test

Direct shear tests were done for silica sand with a relative density similar to that of the sample used in the centrifuge tests. The tests were done at three normal stresses to obtain the friction angle of sand.

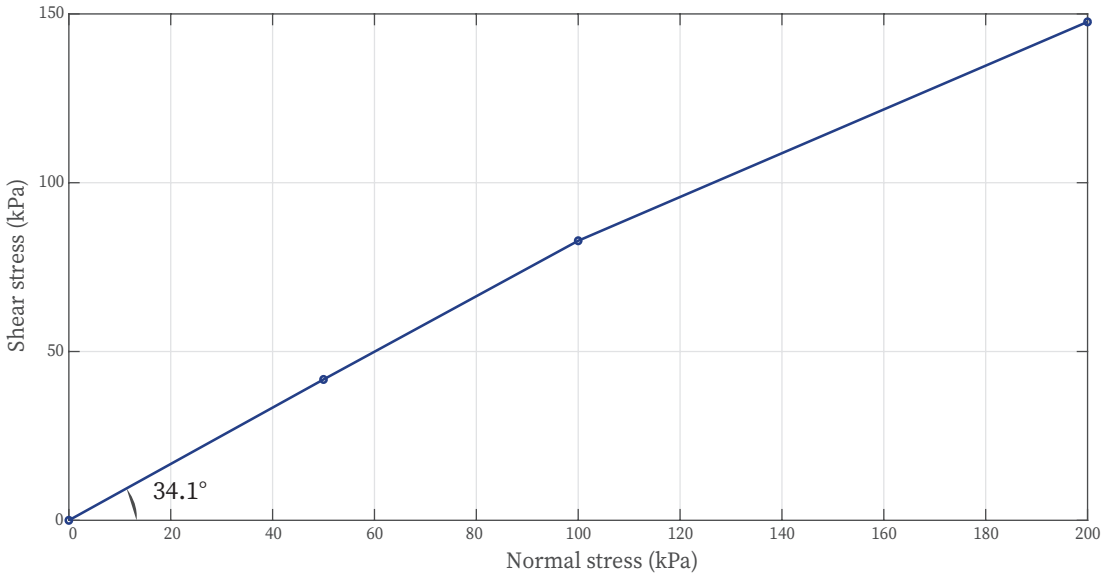

Figure A.1: Plot of Mohr's circle to obtain critical state friction angle from direct shear test

A.2 Sieve analysis

A.2.1 Silica sand

Based on the sieve analysis data provided by the manufacturer, it can be seen that the silica sand used in this research is a fine sand. D_{50} of the sand was 0.390 mm. Uniformity coefficient of the sand was 1.38. It denotes that the sand is uniformly graded. Coefficient of curvature of 1.05 also denotes the same. Grain size distribution curve is given in Figure A.2.

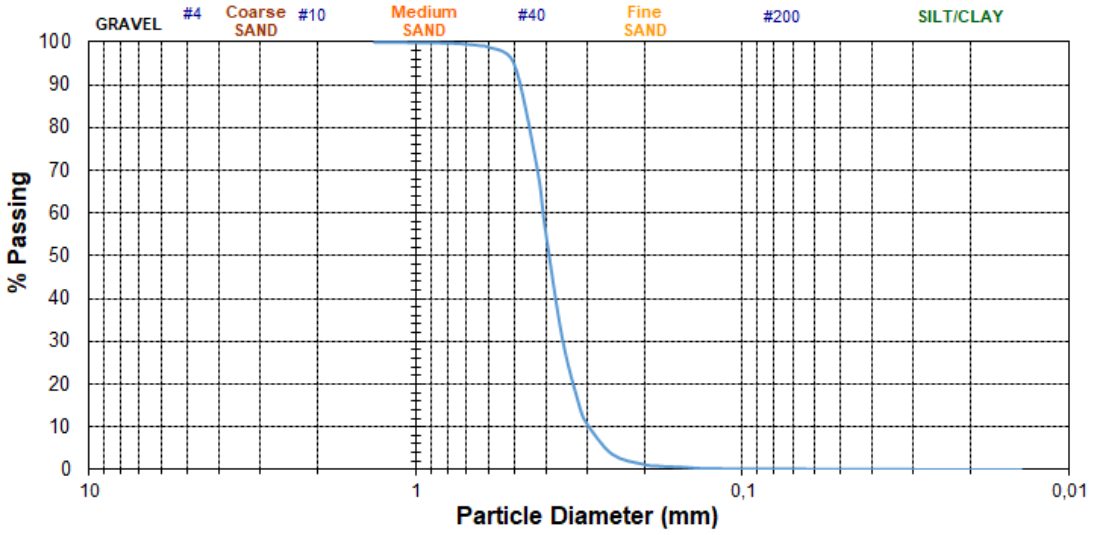

Figure A.2: Grain size distribution curve for silica sand

A.2.2 Geba sand

Sieve analysis data of the geba sand was obtained from A. Maghsoudloo et al (2018) and grain size distribution curve is given in Figure A.3 [23].

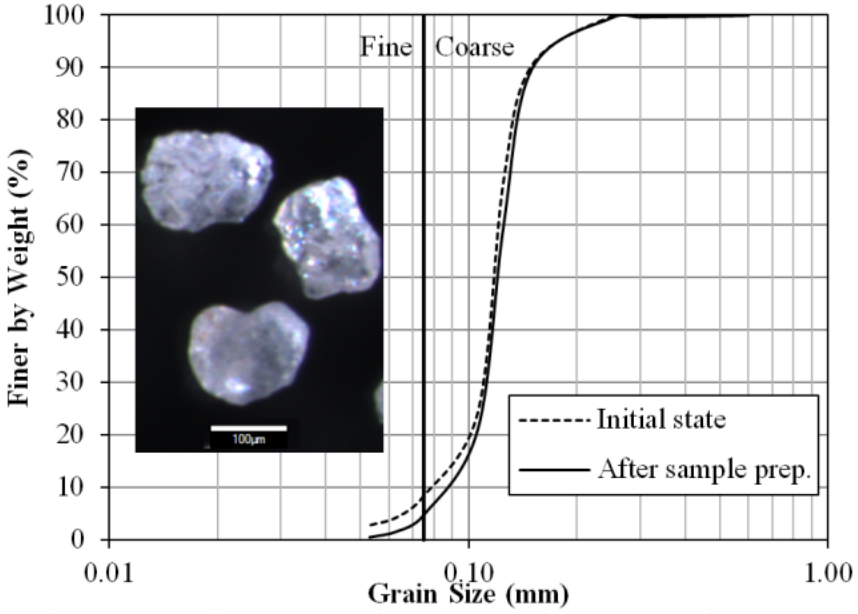

Figure A.3: Grain size distribution curve for geba sand [23]

Appendix B

B.1 Pore pressure behaviour - Frequency effect

In this section, pore pressure behaviour analysis done for the effect of frequency of cyclic loading on homogeneous sand is given. Due to the very low frequency applied in both the tests and also due to use of water as pore fluid in this thesis, minute pore pressures were recorded and this would not have any significant effect on the caisson response to cyclic loading. Higher range of pore pressure values for low frequency loading in negative scale suggests more loosening of sand when compared to high frequency loading.

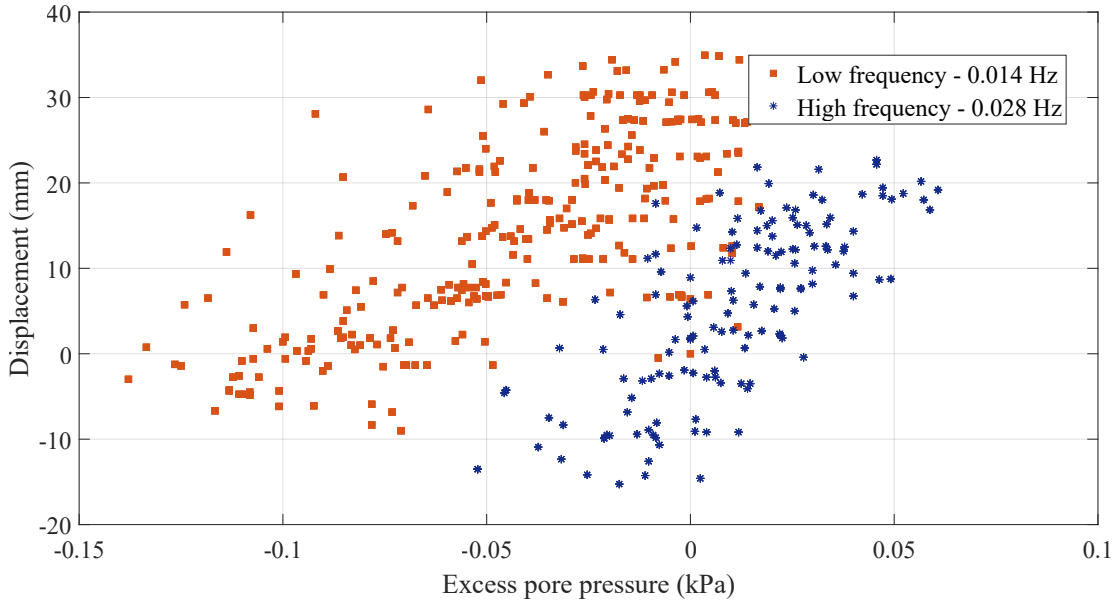

Figure B.1: Suction pressure acquired against the depth of penetration for various tests using fast flow rate

B.2 Installation results

Installation tests done using gravity flow was repeated to gain confidence in the results obtained. Results are presented in Figure B.2.

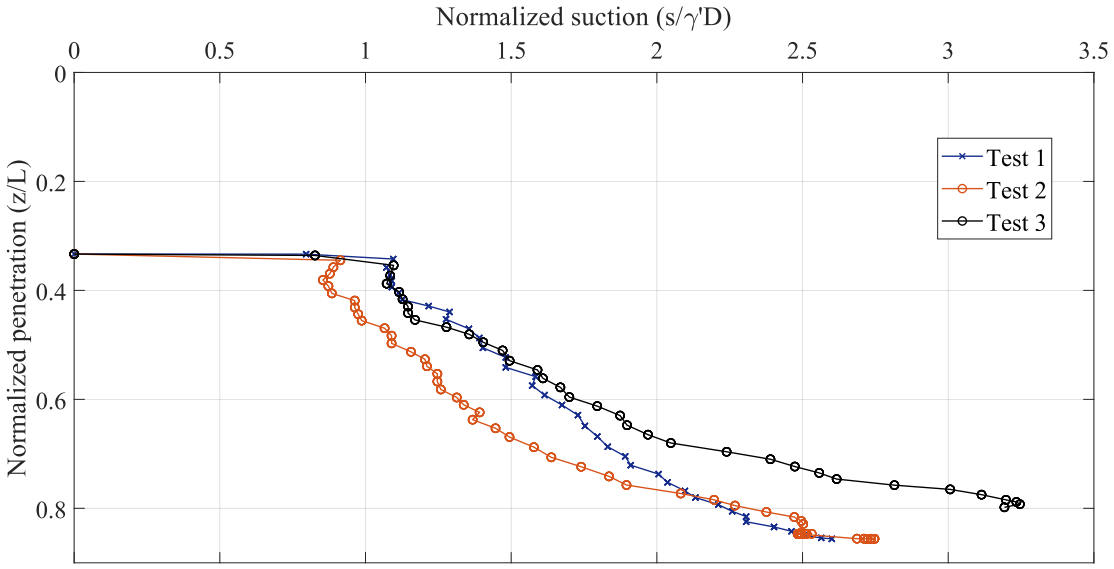

Figure B.2: Suction pressure acquired against the depth of penetration for various tests using fast flow rate

Installation of suction caisson was done to study the behaviour of caissons under cyclic loading. These were done using a fast flow rate using a pump and results are given in the figure below.

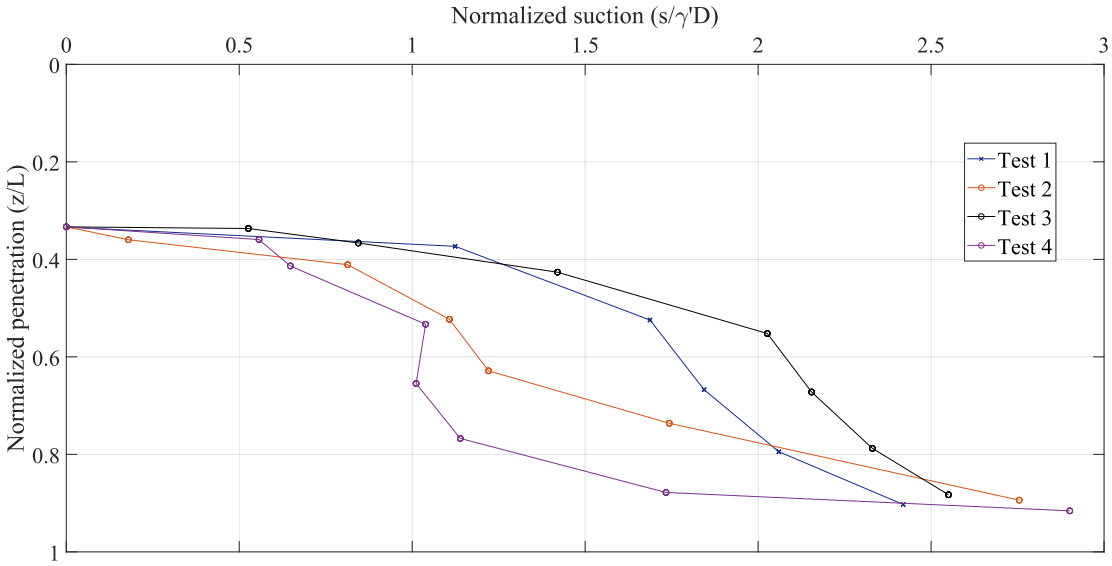

Figure B.3: Suction pressure acquired against the depth of penetration for various tests using fast flow rate

B.3 Cyclic loading tests

Few tests were repeated in the centrifuge to gain more confidence in the physical modelling done in this research. This section presents the displacement plot of the tests repeated in the centrifuge. All the repeated tests showed a behaviour similar to the first test done in the same scenario and thus, results obtained in this research are validated.

B.3.1 One-way compressive loading in homogeneous sand

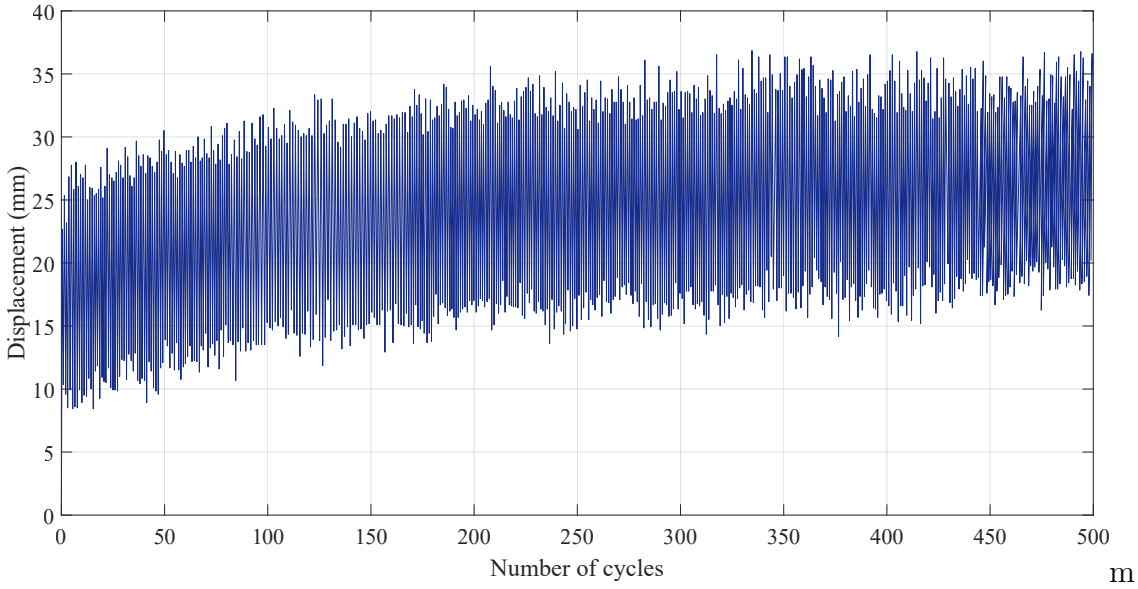

Figure B.4: Settlement behaviour of suction caisson subjected to one-way compressive loading in Homogeneous sand

B.3.2 Two-way symmetric loading in homogeneous sand

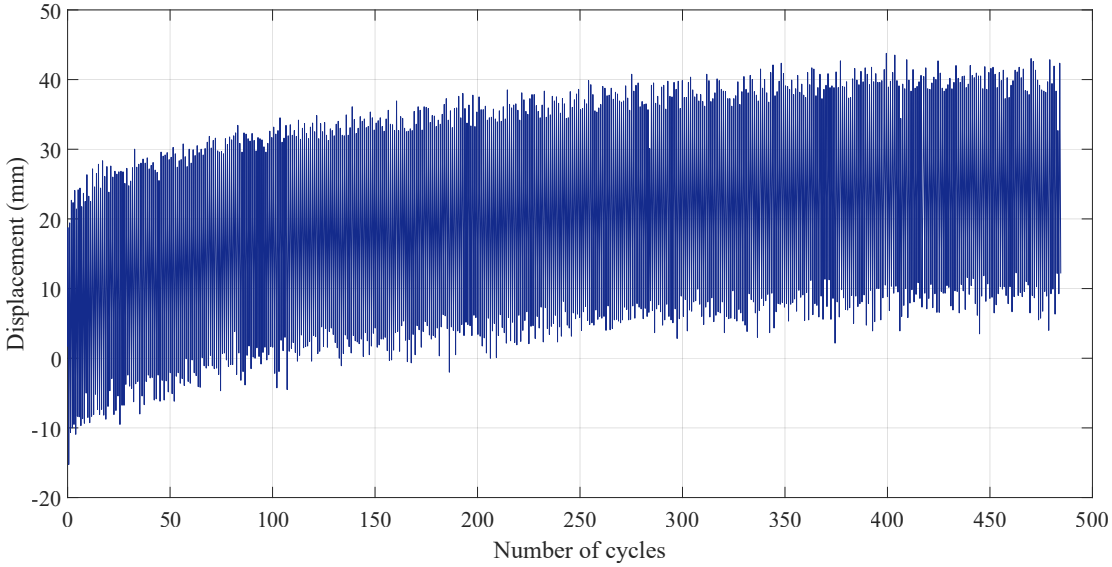

Figure B.5: Settlement behaviour of suction caisson subjected to two-way symmetric loading in Homogeneous sand

B.3.3 One-way compressive loading in layered sand

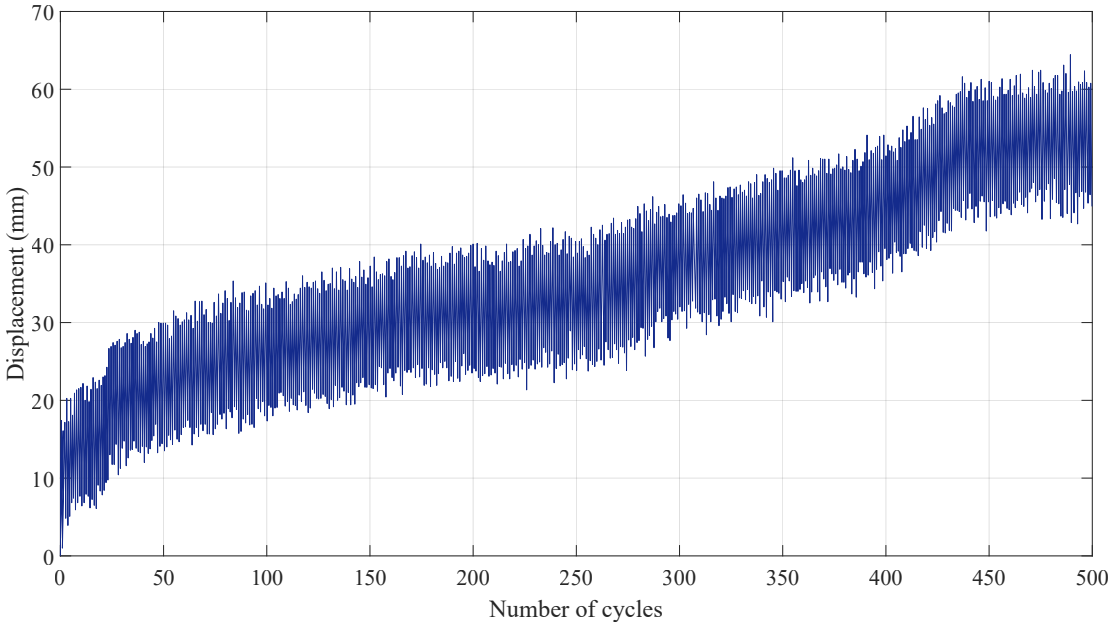

Figure B.6: Settlement behaviour of suction caisson subjected to one-way compressive loading in Layered sand

Appendix C

C.1 Processing centrifuge raw files

Raw data obtained from the centrifuge cyclic loading tests provided very rough plots for each tests. This was a consequence of the interrelated behaviour of the motor in the actuator and the loading rate. Since very low loading rates were used to better control the loading amplitudes, motor did not rotate smoothly. As a result, after each rotation of the motor, motor wheel stopped for a while before proceeding to the next rotation.This caused the plots obtained in the centrifuge to have a teethed shape. To smoothen the centrifuge plots, a matlab code was written, to find the minimum and maximum amplitudes for each cycle along with the corresponding time period. This helped in better visualisation and analysis of the results. Figure C.1 shows the raw centrifuge data and the processed data for a few cycles of one way compressive loading. It can also be noted that the loading amplitudes and the frequency change for every cycle even within the same test due to a slight setback in the feedback loop, but the overall average of maximum and minimum amplitudes of the test provided the desired load amplitude.

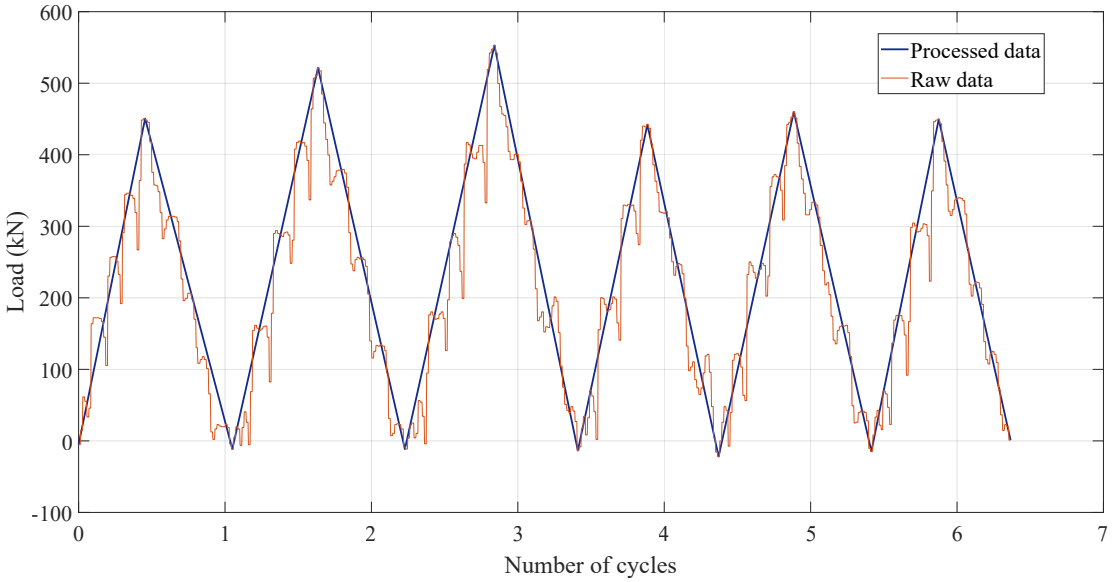

Figure C.1: Processed data vs Raw centrifuge data

C.1.1 Matlab code

```
[num, txt, raw] = xlsread('Suction27080N.xlsx');
time = num(:, 3);
load = num(:, 9);

figure
plot (time, load)

extrema = zeros(1, length(time));
tim = zeros(1, length(time)+length(time)+1);
maximum = zeros(1, length(time));
minimum = zeros(1, length(time));
maxlocs = zeros(1, length(time));
minlocs = zeros(1, length(time));

freq = 35;   %Frequency of cyclic loading

index = 1;
extrema(index) = load(index);
tim(index)  = time(index);
minlocs(index) = time(index);
idx = 2;

while (100*(index)+(freq*10))<length(time)
    if (tim(idx-1)*10+(freq*10))<length(time)
        [maximum(index), i] = max(load(tim(idx-1)*10+1 : tim(idx-1)
           *10+(freq*10)));
        tim(idx) = floor((i + tim(idx-1)*10)/10);
        maxlocs(index) = tim(idx);
    end

    if tim(idx)*10+(freq*10)<length(time)
        idx = idx + 1 ;
        [minimum(index), i] = min(load(tim(idx-1)*10  : tim(idx-1)
           *10+(freq*10)));
        tim(idx) = floor((i + (tim(idx-1)*10))/10);
        minlocs(index) = tim(idx);
    else
        idx = idx + 1 ;
        [minimum(index), i] = min(load(tim(idx-1)*10 : length(time)));
        tim(idx) = floor((i + (tim(idx-1)*10))/10);
        minlocs(index) = tim(idx);
        break;
    end
```

```
42      idx = idx + 1;
43      index = index + 1;
44      disp(index);
45  end
46
47  minlocs(index+1:end) = [];
48  maxlocs(index+1:end) = [];
49  maximum(index+1:end) = [];
50  minimum(index+1:end) = [];
51  tim(idx+1:end) = [];
52
53  index = 2;
54
55  for a = 1: length(tim)
56
57      if a<=length(maximum)
58          extrema(index) = maximum(a);
59          index = index + 1;
60      end
61
62      if a<=length(minimum)
63          extrema(index) = minimum(a);
64          index = index + 1;
65      end
66  end
67
68  extrema(index:end) = [];
69
70  maxavg= mean(maximum)
71  minavg= mean(minimum)
72
73  %Ploting of graphs
74  figure
75  plot(time,load);
76  hold on;
77
78  plot(maxlocs, maximum, 'LineStyle', 'none', 'Marker', 'none');
79  hold on;
80  %
81  plot(minlocs, minimum, 'LineStyle', 'none', 'Marker', 'none');
82  hold on;
83  %
84  plot(tim, extrema);
85  %
86  xlabel('Time (sec)')
```

```
87 ylabel('Load (N)')
88 %Saves the obtained load amplitudes and corresponding time
89 filename = 'Load.xlsx';
90 xlswrite(filename,extrema.');
91 filename = 'Time.xlsx';
92 xlswrite(filename,tim.');
```

Bibliography

[1] M. Senders, "Suction Caissons in Sand As Tripod Foundations for Offshore Wind," *Ph.D. thesis, The University of Western Australia*, 2008. [Online]. Available: http://www.docstoc.com/docs/36120890/SUCTION-CAISSONS-IN-SAND-AS-TRIPOD-FOUNDATIONS-FOR-OFFSHORE-WIND

[2] B. W. Byrne and G. T. Houlsby, "Foundations for offshore wind turbines," *Philosophical Transactions of the Royal Society A: Mathematical, Physical and Engineering Sciences*, vol. 361, no. 1813, pp. 2909–2930, 2003.

[3] "UNFCCC," 2018. [Online]. Available: https://unfccc.int/process-and-meetings/the-paris-agreement/what-is-the-paris-agreement

[4] windeurope.org, "Wind in power 2017," Tech. Rep., 2018. [Online]. Available: https://windeurope.org/wp-content/uploads/files/about-wind/statistics/WindEurope-Annual-Statistics-2017.pdf

[5] "NES Global Talent," 2016. [Online]. Available: https://www.nesgt.com/blog/2016/07/offshore-and-onshore-wind-farms

[6] I. Pineda, "Offshore Wind in Europe WindEurope Business Intelligence Tom Remy (Construction highlights) Ariola Mbistrova (Financing highlights) Courtesy of Øyvind Gravås Statoil-Floating Offshore Wind Farm: Hywind Scotland," Tech. Rep., 2018.

[7] K. Peire, H. Nonneman, and E. Bosschem, "GRAVITY BASE FOUNDATIONS FOR THE THORNTON BANK OFFSHORE WIND FARM," Tech. Rep.

[8] M. N. Tran, "Installation of Suction Caissons in Dense Sand and the Influence of Silt and Cemented Layers," no. October, p. 257, 2005.

[9] L. Bo Ibsen, G. Houlsby, and B. Byrne, "Suction caissons for wind turbines," in *Frontiers in Offshore Geotechnics*, 2005.

[10] T. I. Tjelta, "The suction foundation technology," *Keynotes Frontiers in Offshore Geotechnics III*, pp. 978–1, 2015.

[11] G. T. Houlsby, R. B. Kelly, and B. W. Byrne, "The tensile capacity of suction caissons in sand under rapid loading," *Frontiers in Offshore Geotechnics, ISFOG 2005 - Proceedings of the 1st International Symposium on Frontiers in Offshore Geotechnics*, no. 1, pp. 405–410, 2005. [Online]. Available: http://www.scopus.com/inward/record.url?eid=2-s2.0-72849143924&partnerID=tZOtx3y1

[12] M. Senders and M. F. Randolph, "CPT-Based Method for the Installation of Suction Caissons in Sand," *Journal of Geotechnical and Geoenvironmental Engineering*, vol. 135, no. 1, pp. 14–25, 2009. [Online]. Available: http://ascelibrary.org/doi/10.1061/%28ASCE%291090-0241%282009%29135%3A1%2814%29

[13] G. T. Houlsby and B. W. Byrne, "Design procedures for installation of suction caissons in sand," *Proceedings of the Institution of Civil Engineers - Geotechnical Engineering*, vol. 158, no. 3, pp. 135–144, 2005. [Online]. Available: http://www.icevirtuallibrary.com/doi/10.1680/geng.2005.158.3.135

[14] D. Norske Veritas, "DET NORSKE VERITAS AS Design of Offshore Wind Turbine Structures," Tech. Rep., 2014. [Online]. Available: www.dnvgl.com.

[15] C. Lupea, "Long Term Effects of Cyclic Loading on Suction Caisson Foundations," 2014.

[16] R. B. Kelly, G. T. Houlsby, and B. W. Byrne, "A comparison of field and laboratory tests of caisson foundations in sand and clay," *Géotechnique*, vol. 56, no. 9, pp. 617–626, 2006. [Online]. Available: http://www.icevirtuallibrary.com/doi/10.1680/geot.2006.56.9.617

[17] B. W. Byrne and G. T. Houlsby, "Experimental Investigations of the Response of Suction Caissons to Transient Combined Loading," *Journal of Geotechnical and Geoenvironmental Engineering*, 2004.

[18] R. Brinkgreve, E. Engin, and H. Engin, "Validation of empirical formulas to derive model parameters for sands," in *Numerical Methods in Geotechnical Engineering*, 2000.

[19] "PLAXIS 2D Material Models Manual 2018," Tech. Rep.

[20] A. Tsegaye, "Liquefaction Model (UBC3D)," no. 1, pp. 1–39, 2010.

[21] G. Madabhushi, *Centrifuge Modelling for Civil Engineers*. CRC Press, Taylor & Francis Group, 2015.

[22] "Pumps school," 2017. [Online]. Available: http://www.pumpschool.com/principles/external.asp

[23] R. d. J. F. M. . M. H. A. Maghsoudloo, A. Askarinejad, "Experimental investigation of pore pressure and acceleration development in static liquefaction induced failures in submerged slopes," *Physical Modelling in Geotechnics*, vol. Volume 2, no. Proceedings

of the 9th International Conference on Physical Modelling in Geotechnics (ICPMG 2018), July 17-20, 2018, 2018.

[24] B. Bienen, R. T. Klinkvort, C. D. O'Loughlin, F. Zhu, and B. W. Byrne, "Suction caissons in dense sand, part II: vertical cyclic loading into tension," *Géotechnique*, pp. 1–15, 2018. [Online]. Available: https://www.icevirtuallibrary.com/doi/10.1680/jgeot.16.P.282

[25] D. E. Normandeau and T. F. Zimmie, "The Effect of Frequency of Cyclic Loading on Earth Structures and Foundation Soils," in *International Conferences on Recent Advances in Geotechnical Earthquake Engineering and Soil Dynamics*, vol. 39, 1991. [Online]. Available: http://scholarsmine.mst.edu/icrageesdhttp://scholarsmine.mst.edu/icrageesd/02icrageesd/session01/39

[26] A. . Shajarati, K. W. Sørensen, S. K. Nielsen, and L. B. Ibsen, "Behaviour of Cohesionless Soils During Cyclic Loading," Tech. Rep. 14, 2012.

[27] R. García-Rojo and H. J. Herrmann, "Shakedown of unbound granular material," *Granular Matter*, 2005.